Enhancing turbulent fluctuation measurement with tailored wind lidar profilers

Maxime Thiébaut [1], Frédéric Delbos [2], and Florent Guinot [1]

[1]France Énergies Marines, Technopôle Brest-Iroise, 525 Avenue Alexis de Rochon, 29280 Plouzané, France
[2]Vaisala France SAS, 6A, rue René Razel, Tech Park, CS 70001, 91400 Saclay Cedex, France

Correspondence: Maxime Thiébaut (maxime.thiebaut@france-energies-marines.org)

Abstract. This study ~~separately investigates~~ evaluates the impact of an enhanced sampling rate ~~and reduced probe length on turbulent~~ on turbulence measurements using the Vaisala WindCube v2.1 lidar profiler~~, in comparison to the commercially configured WindCube v2.1. In the first experiment, a tailored lidar sampled~~ . A prototype configuration, sampling four times faster than the ~~standard setup. In the second experiment, a tailored lidar employed a 15 m probe length, compared~~ commercial setup, was compared to the commercial WindCube v2.1 with reference measurements provided by a 2D sonic anemometer mounted on a measurement mast. Over the 47-day experiment, the prototype configuration showed performance similar to the commercial ~~configuration's 23 m. The study offers a detailed analysis of how these changes affect various aspects of wind measurement, including~~ setup for key performance indicators (KPIs) like slope and coefficient of determination of mean wind speed compared to reference measurements, with both configurations meeting "best practice" threshold. However, for mean wind speed ~~, standard deviation, velocity spectra, noise level, integral length scale, and dissipation rate. Increasing the sampling rate improves turbulence measurement without affecting mean wind speed measurement. However, a slight reduction in data availability was observed compared to~~ differences, the commercial configuration met the "best practice" level, while the prototype met the "minimum acceptance" criterion. Additionally, the data availability of the prototype configuration was 0.5% lower than that of the commercial configuration. ~~Reducing the probe length results in higher standard deviation values~~ Moreover, the increased sampling rate in the prototype lidar resulted in higher mean variance in instrumental noise compared to the commercial configuration~~, but this comes at the expense of increased noise levels, making it unclear whether the higher standard deviations are due to the energy of smaller eddies or noise. Additionally, the reduced probe length configuration exhibited a high bias in mean wind speed measurement and had a limited impact on other turbulence metrics. These findings suggest that the best improvement for turbulence measurement with the WindCube lidar profiler is achieved through an increased sampling rate~~. Despite this limitation, the mean noise-corrected along-wind variance measured by the prototype lidar was approximately 7% higher than that of the commercial lidar, suggesting that the prototype might be better at capturing additional turbulent energy by resolving smaller eddies. This effect was especially evident at higher wind speeds. Error metrics for the noise-corrected along-wind standard deviation in the prototype lidar were approximately 25% lower than those of the commercial configuration. However, the observed improvements of the prototype configuration in measuring turbulence fell short of expectations due to inherent limitations in the measurement process within the probe, where spatial and temporal filtering effects constrain the detection of turbulence at certain scales.

1 Introduction

Accurate turbulence data ~~enables~~ enable better understanding and control of wind flow patterns, optimizing the design, operation, and maintenance of wind energy systems. Furthermore, turbulence measurement plays a pivotal role in addressing key challenges within the wind energy sector. It aids in enhancing the efficiency and safety of wind turbine operations, minimizing wear and tear on vital components, and extending the lifespan of these costly assets. Additionally, improved turbulence measurement can facilitate more precise wind resource assessments, aiding in site selection and the overall planning of wind energy projects.

In the wind energy sector, the utilization of wind lidar profiler technology has gained significant traction in recent years, supplanting the traditional meteorological mast equipped with in-situ sensors like cup or sonic anemometers as the standard means of measuring key mean wind properties, such as speed and direction. ~~Lidar~~ Wind lidar profilers present compelling advantages, including the potential for cost reduction compared to meteorological masts and the capacity to measure at similar or even greater heights above the ground.

Wind lidars profilers can be categorized according to their emission waveform, i.e., pulsed or continuous, and measuring technique, i.e., Doppler beam swinging (DBS) (Strauch et al., 1984) or velocity-azimuth display (VAD) (Browning and Wexler, 1968) . Measurement methods used by ~~lidar profiler~~ wind lidar profilers are fundamentally different ~~than~~ from those used by cup or sonic anemometers. Anemometers ~~provide an estimate of the wind speed across a volume of~~ estimate wind speed over a

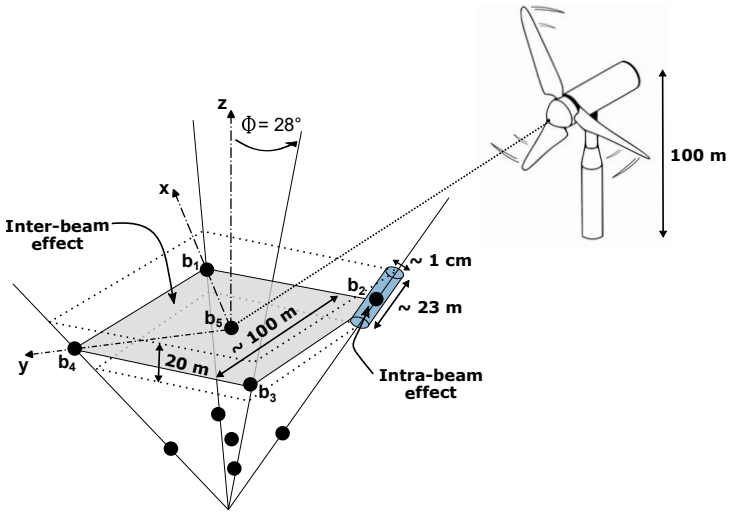

Figure 1. A schematic illustration of inter- and intra-beam effects in the WindCube v2.1 lidar profiler measurement process. The blue cylinder represents the probe volume, corresponding to the dimensions of the commercial lidar configuration. The positions of the five beams are labeled as b_i, where i ranges from 1 to 5. The inclination of the diverging beams (from beam 1 to beam 4) with respect to the vertical z-axis is $\phi = 28^\circ$. Beam 5 is aligned with the z-axis, while beams 1 and 3 are aligned with the x-axis, and beams 2 and 4 are aligned with the y-axis in the coordinate system of the instrument, as stipulated by the manufacturer.

small volume of just a few cubic centimeters~~whereas lidars~~ , whereas pulsed lidar profilers provide an average ~~across a probe volume of up to several dozen cubic meters . Lidars can be categorized according to their emission waveform, i.e., pulsed or continuous, and measuring technique, i.e., Doppler beam swinging (DBS)(Strauch et al., 1984) or velocity-azimuth display (VAD) (Browning and Wexler, 1968)~~over a cylindrical probe several dozen meters long with a cross-sectional diameter of less than 1 cm (Fig. 1).

However, wind lidar profilers have yet to garner widespread acceptance for turbulence measurement, which remains a focal point of ongoing research. In contrast to turbulence data derived from reference instruments such as sonic anemometers, turbulence data ~~derived~~ from lidar profiler measurements suffer from systematic errors induced by ~~,~~ (i) ~~,~~ the inter-beam effect, also known as the cross-contamination effect, (ii) ~~,~~ the intra-beam effect, ~~i.e~~i.e., the averaging effect of the probe volume ~~, (iii) , low sampling rate~~ (Fig. 1) and, ~~(iv), noise.~~ iii), instrumental noise.

The inter-beam effect can ~~lead to~~ result in either underestimation or overestimation of turbulence metrics~~(Kelberlau and Mann, 2020) . This discrepancy arises~~ , arising from the modulation of energy associated with eddies ~~characterized by specific wavenumbers .~~ of specific wavenumbers (Kelberlau and Mann, 2020). Any phase difference between the horizontal and vertical components of an eddy significantly impacts the filtering of flow structures, potentially leading to both amplification or attenuation of their measured turbulent energy (Theriault, 1986; Gargett et al., 2009).

The intra-beam effect ~~is a consequence of the probe length, effectively acting as a low-pass filter. This phenomenon stems from the filtering out of eddies that fall beneath the size threshold set by the probe length, generating underestimation of turbulence metrics.~~ generates underestimation of turbulence metrics. It arises from two anisotropic filtering processes: (1) spatial filtering due to averaging over the probe volume and (2) temporal filtering caused by averaging over the beam's pulse accumulation time, Δt, at a given measurement position. These two effects give rise to a transfer function, H, applied by the instrument on the signal measured within the probe. The transfer function includes a part due to time-averaging (the sinc term) and a part due to space-averaging (the Gaussian term), such that (e.g., Kristensen et al., 2011):

~~Lidar~~

$$|H|^2(\mathbf{k}) = \mathrm{sinc}^2\left(\frac{\Delta t}{2}\mathbf{k}\cdot\mathbf{U}\right)\exp\left(-\left[\sigma_l^2(\mathbf{k}\cdot\mathbf{b})^2 + \sigma_r^2(\parallel\mathbf{k}\parallel^2 - (\mathbf{k}\cdot\mathbf{b})^2)\right]\right) \quad (1)$$

Here, $\mathbf{k}$ is the turbulent structure wavevector, $\mathbf{b}$ is the beam pointing vector, $\mathbf{U}$ is the vector associated with the wind direction of magnitude U, and σ_l and σ_r represent the Gaussian weighting factors in the along-beam and cross-beam directions, respectively.

From Eq. 1, it follows that wind field structures with wavelengths smaller than σ_l in the along-beam direction are attenuated, as are those with wavelengths smaller than σ_r in the cross-beam direction. However, in the latter case, these structures are so small that the filtering effect becomes negligible, as the cross-section of the probe is approximately 1 cm (Fig. 1). Ultimately, assuming the Taylor frozen turbulence hypothesis, the wavevector domain that passes through the filter is defined by the intersection of two slices: one perpendicular to the direction of $\mathbf{U}$, which preserves structures longer than $\pi\Delta t U$, and another perpendicular to the direction of $\mathbf{b}$, which retains structures longer than σ_l. All other structures are filtered out.

Pulsed lidar profilers require several seconds to complete a full scanning ~~circle,~~ cycle resulting in a low sampling rate that causes discrepancies between turbulence measurements taken by anemometers and those by lidar profilers (e.g., Peña et al., 2009). ~~Turbulent motion scales can~~ While the sampling rate governs how quickly the lidar progresses through a scan cycle, it is directly influenced by pulse accumulation time. Consequently, even if the sampling rate is increased, pulse accumulation can still limit the ability of the lidar to resolve small-scale turbulent structures. Since turbulent motion scales vary from milliseconds to hours and from centimeters to kilometers (e.g., Stull, 2000), ~~but lidars are limited to measuring turbulent motions with timescales of seconds and spatial scales of tens of meters. However, wind turbine components are influenced by various scales of turbulent structures, making it crucial to detect a broad range of smaller turbulence scales~~it is crucial to account for both temporal and spatial filtering effects when assessing lidar-based turbulence measurements.

The concept of measuring turbulence using remote sensing instruments has gradually evolved since the early works in radar meteorology by Lhermitte (1962) and Browning and Wexler (1968). Lhermitte (1969) was the first to propose a method for inferring turbulence by analyzing the variance of radial velocity measurements through VAD scanning. Following this, Wilson (1970) conducted pioneering experiments using a pulsed Doppler radar to detect turbulence within the convective boundary layer (0.1-1.3 km). However, these early measurements were limited to turbulence scales larger than the pulse volume and smaller than the scanning circle, and no validation against reference instruments was performed, questioning their reliability.

Kropfli (1986) expanded Wilson's approach to capture turbulence scales larger than the scanning circle by integrating data from multiple scans. Although initially developed for Doppler radar, these methods were later adapted for Doppler lidar. Eberhard et al. (1989) were the first to apply Wilson's and Kropfli's methods using lidar, and Gal-Chen et al. (1992) further refined the technique with a different scanning configuration. Despite these advancements, the significant probe length (around 100 m) limited studies to the convective boundary layer due to considerable probe volume averaging, especially near the ground. To address this limitation, research shifted towards understanding and mitigating probe volume averaging effects (e.g., Smalikho et al., 2005; Mann et al., 2010; Branlard et al., 2013). Nowadays, modern lidar systems have reduced probe lengths to about 30 m, but averaging effects still pose challenges for turbulence measurements in the surface layer where wind turbines operate (e.g., Mann et al., 2009; Sjöholm et al., 2009; Sathe et al., 2011; Sathe and Mann, 2012).

~~Considering the pivotal role of turbulence measurement in wind energy applications, the past decade has seen significant advancements in the development and customization of wind lidar technology. Notably, a study by Sathe et al. (2015) proposed a novel six-beam method for measuring turbulence using a Vaisala pulsed lidar Windcube 200. This method involves capturing line-of-sight (LOS) velocity fluctuations at five equally spaced azimuth angles along the base of a scanning cone and a sixth measurement at the center of the scanning circle using a vertical beam at the same height. When compared to the traditional VAD method, which often results in significant averaging effects on measured turbulence, the six-beam approach offers improved accuracy. Specifically, the six-beam method was found to measure 85-101% of the reference turbulence indicated by a cup anemometer, whereas the VAD method measured only 66-87% of the reference turbulence, depending on atmospheric stability and the wind field component.~~

The present paper ~~aligns with this trajectory, as it~~ delves into the specific advancements pertaining to the Vaisala WindCube v2.1 lidar profiler. ~~Two key modifications are explored: first,~~ A key modification is explored: an augmentation of the sampling

rate, ~~and second, a reduction in the probe length. These customizations are individually evaluated for their~~ achieved by reducing the pulse accumulation time. This customization is evaluated for its impact on the measurement of mean wind ~~statistics such as the mea, wind speedand turbulent metrics such as the standard deviation of wind velocity, the velocity spectra, the vertical integral length scale and the dissipation rate~~speed, data availability, and along-wind variance and standard deviation. The impact of ~~noise on both modifications~~ instrumental noise on this modification is also evaluated ~~. Notably, this study does not address the combined effects of both modifications.~~ to demonstrate that the potential improvement in turbulence estimates with the version featuring increased sampling rate is not due to noise.

2 Data and methods

2.1 ~~Modifications to the WindCube v2.1 lidar system~~Prototype configuration with increased sampling rate

2.1.1 ~~Increased sampling rate~~

The WindCube v2.1 lidar ~~profiler employs a DBS technique for measuring~~ is designed for general atmospheric measurements, such as mean wind speed and direction, requiring a careful balance between temporal resolution, spatial resolution, and carrier-to-noise ratio (CNR). Its default sampling rate is optimized to ensure high data quality and availability across varying altitudes and atmospheric conditions while maintaining system efficiency and manageable data processing.

The WindCube v2.1 employs the Doppler Beam Swinging (DBS) technique to measure wind speed. This ~~technique involves the use of~~ method utilizes an optical switch ~~to alternately direct~~ that sequentially directs the lidar beam ~~in the~~ toward four cardinal directions (~~north, east, south, and west~~0°, 90°, 180°, and 270° from True North), each ~~at an inclination angle of 28°~~ inclined at $\phi = 28°$ from the vertical. ~~Subsequently, the~~ A fifth beam is directed vertically upwards, ~~providing measurements from a total of~~ resulting in wind measurements at five distinct positions (Fig.~~1a).~~ 1-2).

In its standard commercial configuration, the WindCube lidar collects data at each ~~location in 1 second and steers the beam~~ position for approximately $\Delta t = 0.8$ seconds before switching to the next~~location. This process completes a full DBS scan~~. Including transition times, a complete DBS scan is performed in 4 seconds, ~~resulting in a~~ yielding a line-of-sight (LOS) velocity sampling rate of 0.25 Hz~~for LOS velocity and 1 Hz for wind speed.~~

~~These frequencies are~~ . This sampling rate is well-suited ~~to capture turbulent structures with dimensions of~~ for capturing turbulent structures larger than 100 ~~m and beyond~~meters. However, ~~it's worth noting that~~ wind turbine components ~~are affected by turbulent structures across various scales. As a result, it becomes essential to increase the lidar profiler's sampling rate to encompass a more comprehensive velocity spectrum , enabling the capture of turbulence structures at smaller scales that also impact wind turbine components~~experience loads from turbulence across a wide range of scales. Increasing the sampling rate is crucial for broadening the velocity spectrum captured by the lidar, potentially enabling the detection of smaller-scale turbulence that influences turbine performance.

Theoretically, a higher sampling rate improves temporal resolution and extends the resolved turbulence frequency range. However, for wind lidar profiler technology, this enhancement comes with trade-offs. The duty cycle, which represents the

proportion of time the lidar transmits pulses, decreases as sampling rate increases, potentially reducing signal strength. Moreover, increasing the sampling rate requires a reduction in accumulation time, resulting in fewer pulses per sample and increasing noise. The default WindCube v2.1 configuration balances these factors to maximize data reliability. It integrates a high number of pulses per measurement to enhance signal quality, making it well-suited for general wind resource assessment. However, its probe length of approximately 23 meters (Fig. 1) limits its ability to resolve small eddies compared to point sensors like sonic anemometers.

In response to the demand for ~~increased sampling rate, we have engineered a tailored iteration~~ capturing the energy of smaller eddies, we developed a modified version of the WindCube v2.1 ~~. This enhanced version~~ that operates four times faster, ~~providing~~ achieving a LOS velocity ~~and wind speed~~ sampling rate of 1 Hz~~and 4 Hz respectively. This improvement~~ . This modification was achieved by reducing the accumulation time for data collection from each beam ~~by 70%,~~ in conjunction with a ~~corresponding 70%~~ reduction in the number of transmitted pulses. ~~Please note that specific details regarding the accumulation time and pulse count cannot be disclosed publicly.~~

~~The dataset used to assess the impact of the increased sampling rate on the measurement of turbulent fluctuations encompasses a 47-day period, split into 2256 30-min subsets, spanning two time intervals: from November 12 to November 25, 2021, and from December 7, 2021, to January 10, 2022. During this campaign, lidar measurements were recorded at ten different heights ranging from 40 to 200 m above ground level. This measurement campaign was conducted as part of the lidar test verification performance at the Janneby site , Germany, overseen by DNV-GL. The commercial lidar configuration and a prototype version with an enhanced sampling rate, positioned approximately 14 m apart, were tested against a meteorological mast equipped with cup and sonic anemometers. Both configurations successfully passed the test. Please note that this paper does not discuss~~

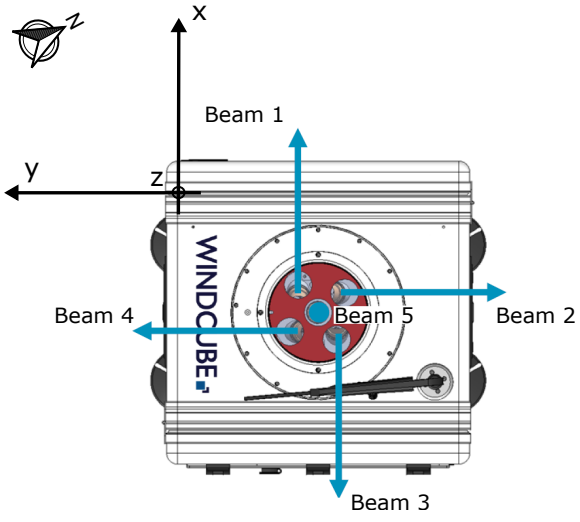

Figure 2. Top view of a WindCube v2.1 lidar showing the positions of its five beams. The x-axis is oriented from beam 3 towards beam 1, the y-axis extends from beam 4 towards beam 2, and the vertical z-axis points upward along beam 5. The arrow indicates North. For the present study, the primary x-axis of the lidars was oriented at -62° relative to North.

the measurements obtained from the anemometers. Schematic illustration of inter and intra-beam filtering effects in WindCube v2.1 lidar profiler measurement process. The blue cylinder represents a probe with dimensions matching the commercial lidar configuration.

Length, Δz, of the probe is expressed as a function of pulse length, T, and speed of light, c.

2.1.1 Reduced probe length

The intra-beam filtering effect factor of 4 was chosen as a compromise between increasing temporal resolution and maintaining an acceptable CNR and data availability. This choice is intended to keep wind measurements comparable to those from the commercial configuration while enabling the investigation of smaller-scale turbulence. The actual impact on measurement performance will be assessed in the study.

2.2 Field measurement

2.2.1 Measurement site and data collection

The field measurement campaign was carried out by DNV-GL at the lidar validation test site in Janneby, Germany (Fig.1)is a result of the probe length, which effectively acts as a low-pass filter by selectively attenuating eddies smaller than the probe length. This phenomenon occurs because it filters out eddies smaller than the size threshold defined by the probe length, denoted as Δz (with units of length). The pulse length (with units of time), T, determines the probe length, and in the case of the WindCube v2.1 lidar, multiple pulses are sent into the atmosphere. Each pulse occupies a volume in the atmosphere at time t, defined by $\Delta z = cT/2$, where c represents the speed of light 3). Due to its flat terrain, the site features orography-undisturbed flow, which is suitable for the verification trials of lidar systems. The site has relatively good exposure to largely undisturbed wind conditions, i.e., undisturbed winds from almost all sectors. The elevation of the site is a few meters above mean sea level, and the surface roughness is low due to the primarily agricultural land use (Fig.**??**).

In its standard commercial configuration, the WindCube v2.1 measures LOS velocity within a probe of approximately 23 m (Fig. 1). This corresponds to acertain Transistor-Transistor Logic (TTL) pulse duration, the specific value of which cannot be publicly disclosed. The tailored version of the WindCube v2.1 lidar features a 50% reduction in pulse duration, leading to a reduction in the probe length from 23 m to 15 m. 3a). Two wind turbines (WT N100 and WT N117 in Fig. 3a) are installed in the vicinity of the meteorological mast. The closest wind turbine is located 210 m from the mast. A few human constructions (houses, sheds), not exceeding 15 m in height, are located approximately 500 m southwest of the mast.

The dataset used to evaluate the impact of the reduced probe length on the measurement of turbulent fluctuations spans 4 days, from May 31, 15:00 (UTC 0) to June 04, 15:00 (UTC 0), 2023, divided into 240 30-minute subsets. Throughout this observational campaign, both the commercial and tailored lidar systems, separated by less than 1 m , collected data at ten distinct heights, ranging from 40 m to 200 m above the lidar instruments. These measurements were conducted on the experimental terrace, located atop the Vaisala office in Saclay, France. The commercial lidar was a "Golden Lidar", meaning it is a reference lidar that has been verified against an IEC-compliant met mast by a third party.

2.3 Evaluation metrics

Our investigation is centered around evaluating the impact of two key enhancements on the WindCube v2.1 lidar profiler: (1) increasing the sampling rate and (2)reducing the probe length. We conduct two distinct measurement campaigns, each focusing on a single enhancement at a time. To establish a baseline, we gather meteorological mast is a 100 m, 3-fold guyed lattice tower with a constant face width of 0.4 m. It is equipped with six MEASNET-calibrated Thies First Class Advanced cup anemometers (No. 4.3352) and a Thies 2D sonic anemometer (No. 4.3830). However, only the Thies 2D sonic anemometer is used in this study to provide reference measurements of mean wind speed and turbulencemeasurements using the commercially configured WindCube v2.1 system. These initial measurements serve as a reference point against which we can effectively assess the effects of the enhancements in both increased sampling rate and reduced probe length., as the cup anemometers data are not available. The mounting arrangements are consistent with the currently valid IEC and IEA recommendations for the use of anemometry at meteorological masts. As shown in Fig. 3b, the sonic anemometer is pointing towards 150° from True North and is mounted at 97 m above ground, which corresponds to the average hub height of modern land-based wind turbines. The sonic anemometer was set to record continuous horizontal wind speed and direction at sampling rates of 4 Hz.

Our study commences by analyzing the effects of the lidar enhancements on the 10-minute average wind speed, U, and data availability. Subsequently, we shift our focus to turbulence analysis, derived from 30-minute subsets of data.

2.2.1 Standard deviation

In this study, we focus on analyzing velocity fluctuations as the primary turbulence metric, quantified through the calculation of standard deviation. Assessing the standard deviation of wind velocity fluctuations is essential in wind energy applications. It offers insights into turbulence intensity, aids in estimating dynamic loads on turbine components, enhances power prediction models, informs turbine control strategies, and supports site assessment for optimal wind farm development and operation.

The standard deviation of the mean velocity along and across the wind propagation, denoted as σ_u

Adjacent to the measurement mast, both the commercial lidar configuration, and σ_v respectively were quantified in this study. To achieve this, we first rotate the velocity measured along the lidar's a prototype version with an enhanced sampling rate were installed 3 m and 13 m apart the mast respectively. The prototype configuration was set to record the LOS velocity four times faster than the commercial configuration, as described in Section 2.1.1. The lidar was aligned such that beams 1 and 3, which correspond to the x-axis , denoted as V_x and aligned with true North , such that the mean velocity along the y-axis, noted as V_y, becomes 0. The wind velocity along (Fig. 2), were oriented at -62° from True North (Fig. 3). According to the manufacturer's recommendation, the x-axis is then aligned with the 30-minute mean wind direction. The expressions for V_x and V_y are given by Eq. **??** and **??**: the primary axis and should be oriented relative to North. Beams 2 and 4 are fixed along the y-axis.

$$V_x = \frac{b_3 - b_1}{2\sin\phi}$$

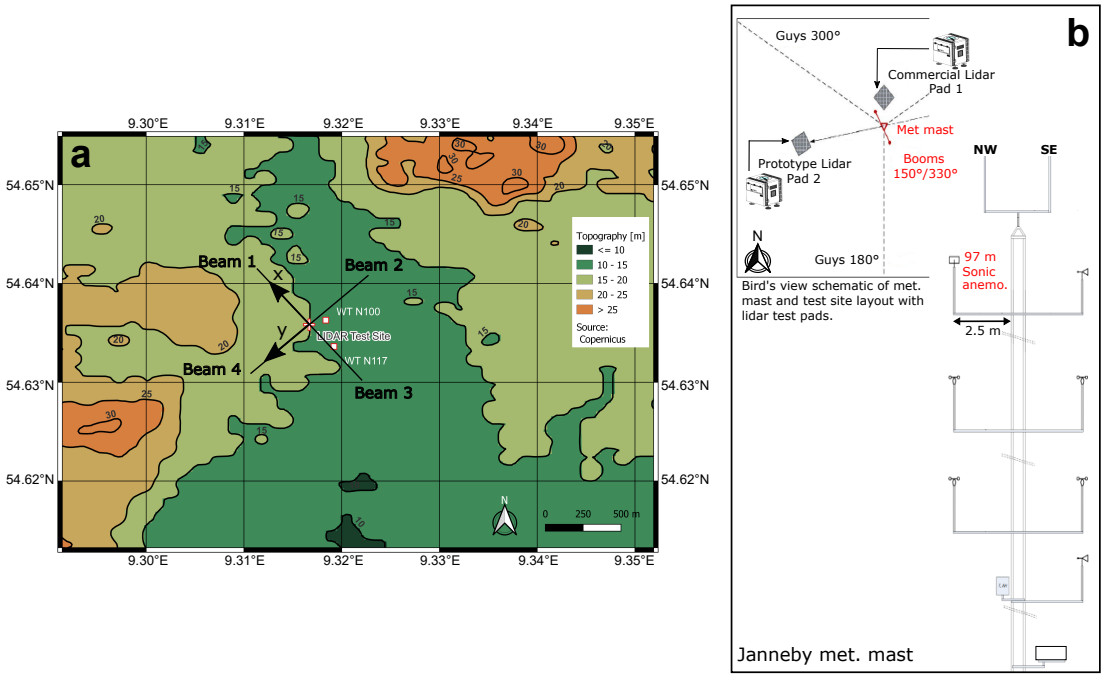

Figure 3. a: Test site location at Janneby, Germany. Black lines indicate the beam orientations for the commercial and prototype configurations. The x and y axes of the instrument coordinate system (see Fig. 2) are marked with black arrows. b: Configuration of the meteorological mast, showing the position of the sonic anemometer. NW and SE denote the north-west and south-east directions. The schematic in panel b also provides a bird's-eye view of the meteorological mast and test site layout, including the lidar test pads.

$$V_y = \frac{b_4 - b_2}{2\,\sin\phi}$$

Here, $\phi = 28°$ represents the zenith angle, and b_i denotes the LOS velocity measured by each beam i, with positive velocity directed towards the instrument.

Furthermore, we investigate the standard deviation, σ_5, of the mean vertical velocity, through direct measurement of the vertical component of the wind speed provided by beam 5.

2.2.1 Integral length scale

Understanding the integral length scale helps in quantifying the spatial extent of turbulence within a wind field. This information is essential for assessing the potential impact of turbulence on the performance and structural integrity of wind turbines. Moreover, integral length scale data is often used as input for turbulence models employed in wind energy simulations. These models help predict wind turbine loads, fatigue, and power output by accounting for the effects of turbulence on the flow fieldThe field measurement campaign was conducted over two periods: from 12 to 25 November 2021, and from 07 December

2021 to 10 January 2022. These two measurement periods were combined to form a 47-day dataset. To facilitate a comparison of turbulence measurements, the sonic-derived wind dataset was resampled to match the sampling rate of the LOS velocities measured by the prototype configuration. This ensures that similar turbulence time scales are captured when calculating and comparing turbulence estimates. Therefore, the sonic anemometer measurements were resampled at 1 Hz.

The ~~5-beam configuration of the WindCube v2.1 lidar enables the computation of the vertical integral length scale, denoted as L_w, propagating along the horizontal flow trajectory, through direct measurements of the vertical velocity by beam 5. However, quantifying the along and across-wind integral length scales, i.e., L_u~~ 47-day dataset was divided into 2256 subsets of 30-minute data records, with each subset containing 450 and ~~L_v respectively, requires wind alignment with one pair of opposite beams.~~

~~The integral length scale, L_j, associated with the direction j can be estimated by calculating the integral timescale, Λ_j. The latter serves as a measure of the duration during which the largest eddies maintain correlation. For each~~ 1800 measurement points for wind data acquired at sampling rates of 0.25 Hz and 1 Hz, respectively. The choice of a 30-minute ~~interval, Λ_j is computed from a temporal autocorrelation function, $R_{jj}(\tau)$, integrated over time from $\tau = 0$ to the first instance of $R_{jj} = 0$ (e.g., Tritton, 2012). For the example of the vertical wind component, the integral timescale, Λ_w, is given by :~~ window deviating from the standard 10-minute window typically used in the wind energy industry was informed by considerations of reduction of random errors in turbulence measurements, as discussed by Lenschow et al. (1994).

~~$$\Lambda_w = \int_{\tau=0}^{\tau[R_{ww}(\tau)=0]} R_{ww}(\tau)\mathrm{d}\tau$$~~

~~with the temporal autocorrelation function defined as:~~

~~$$R_{ww}(\tau) = \frac{R[b_5'(t), b_5'(t+\tau)]}{\sigma_{b_5}^2}$$~~

~~where the prime denotes a fluctuation from the mean. The integral length scale, L_w, is estimated by invoking Taylor's frozen turbulence hypothesis:~~

~~$$L_w = \Lambda_w U$$~~

2.2.1 ~~Velocity spectra~~

2.3 Velocity spectra

Power spectral density of the velocity, i.e., the velocity spectra, provide valuable information about the distribution of turbulent kinetic energy across different scales of motion within the wind flow. This understanding helps in characterizing turbulence and its effects on wind turbine performance and structural loads.

Velocity spectra were computed using Welch's method (Welch, 1967). This method computes an estimate of the spectrum by dividing the data into overlapping segments, computing a modified periodogram for each segment and averaging the periodograms. The Hann window with 50% overlap was applied to each segment to reduce spectral leakage and improve frequency resolution. The 50% overlap is a reasonable trade off between accurately estimating the signal power, while not over counting any of the data.

~~Velocity spectra $S_5(f)$, of the~~ Following the recommendations of Kelberlau and Mann (2020), turbulence velocity spectra computed from the lidar-derived reconstructed velocity component should not be fitted to turbulence models. This is due to the inter-beam effect, which distorts the spectra, rendering them physically meaningless. Therefore, such spectra were not considered in this study. The focus was on velocity spectra $S_i(f)$ derived from the LOS velocities measured by beam ~~5~~ i. The primary limitation in this approach is the intra-beam effect. Spectra were computed for each ~~30-min subsets. The spectra~~ 30-minute subset of data.

The spectra, $S_i(f)$, were fitted by a parametric expression (Teunissen, 1980; Olesen et al., 1984; Tieleman, 1995) in the frequency domain f, to which we add a component ~~N_5~~ N_i associated with the power spectral density of instrumental noise of the LOS velocity measured by beam ~~5~~ i (see section 2.4):

$$S_{5i}(f) = \frac{m}{(1+nf)^{\beta}} + N_{5i} \tag{2}$$

The coefficient m primarily controls the vertical scaling or amplitude of the spectum whereas n influences the rate at which the function decays as f increases. The exponent β determined the shape of the spectrum.

2.3.1 ~~Noise~~

Three different weighting schemes were considered: an unweighted scheme, a low-frequency weighted scheme with weights proportional to the logarithm of the frequency, and a high-frequency weighted scheme with weights inversely proportional to the logarithm of the frequency. Assessing the fitting accuracy included comparing the variance obtained from the integrated fitted spectra with the measured spectra, and calculating their absolute relative differences.

2.4 Instrumental noise

~~Doppler noise is~~ Lidar measurements are inherently influenced by signal noise and potential variations in aerosol fall speeds, both of which contribute additional terms to the observed variance. Assuming that all atmospheric flow contributions to the observed LOS velocity variance within the considered short timescales are of a turbulent nature, the variance $\sigma^2_{b_i}$ of the LOS velocity measured by beam i, can be expressed as the sum of three independent terms (Doviak and Zrnic, 1993):

$$\sigma^2_{b_i} = \sigma^2_{p_i} + \sigma^2_{n_i} + \sigma^2_{d_i} \tag{3}$$

Here, $\sigma^2_{p_i}$ represents the net contribution from atmospheric turbulence at scales measurable by the lidar (Brugger et al., 2016), $\sigma^2_{n_i}$ denotes the variance associated with instrumental noise, and $\sigma^2_{d_i}$ accounts for the variance caused by variations in aerosol

terminal fall speeds within the measurement volume. However, σ_d^2, can typically be neglected, as particle fall speeds are generally less than 1 cm/s (e.g., Bodini et al., 2018). Noise will be identified through two different methods: a spectral approach and an autocorrelation approach, as accurately identifying the variance of noise is critical to our study.

2.4.1 Spectral method

Instrumental noise is a critical factor in the spectral analysis of velocity time series. ~~This type of noise arises from random fluctuations in the frequency of a signal due to the relative motion between the source and the observer.~~ In the spectrum of a velocity time series, ~~Doppler~~ this noise typically manifests as a flattening of the spectrum at higher frequencies, indicating a white noise characteristic that contributes equally across these frequencies (e.g., Thomson et al., 2012; Durgesh et al., 2014; Guerra and Thomson, 2017; McMillan and Hay, 2017; Thiébaut et al., 2020a). At lower frequencies, the spectrum is usually dominated by the actual signal, which may show a characteristic decay or specific features related to the physical process being measured, such as turbulence. As frequency increases, the influence of ~~Doppler~~ the instrumental noise becomes more prominent, leading to a flattened spectral region where the noise dominates.

In Eq. 2, ~~N_5~~ N_i represents the constant ~~Doppler noiselevel~~power spectral density of noise, which contributes to the spectral flattening observed at higher frequencies. ~~This understanding is particularly important in the context of turbulence measurement, where accurately distinguishing between the actual turbulent signal and noise is crucial for comprehending the dynamics and energy distribution within a turbulent flow. Doppler noise can obscure the true signal at higher frequencies, complicating the analysis and potentially leading to erroneous conclusions if not properly accounted for. Failure to account for this noise can result in an overestimation of turbulence metrics such as the dissipation rate (Bodini et al., 2018).~~ The variance of the noise depends on the technical characteristics of the device measuring the velocity, such as Nyquist velocity, the signal spectral width, the number of pulses and points per range gate, and the signal-to-noise ratio. Theoretical expressions for the variance of this noise can be derived and subsequently removed from the computed turbulence metrics to improve accuracy ~~(O'Connor et al., 2010; Bodini et al., 2018, 2019; Wildmann et al., 2019)~~(Pearson et al., 2009; O'Connor et al., 2010; Bodini et al., 2018, . However, the technical specifications of lidar profilers are no longer openly shared with users, making it impossible to evaluate this noise theoretically. ~~Therefore~~To address this, it is ~~necessary to determine this noise using a spectral approach~~essential to evaluate the noise using an alternative method, such as the ~~one presented in this paper.~~

2.4.2 ~~Dissipation rate~~

~~The dissipation rate, ε, quantifies the rate at which turbulent kinetic energy is converted into thermal energy within the atmosphere. Measuring dissipation is crucial for validating atmospheric circulation models, which are essential for accurate wind resource assessments. By providing detailed information about turbulence within the wind flow, the dissipation rate helps improve the precision of these models. This leads to better predictions of wind patterns and energy potential, ultimately enhancing the planning and optimization of wind farms~~spectral approach employed in this study. This approach is comparable to the method proposed by (e.g. Richard et al., 2013; Durgesh et al., 2014). It enables the determination of the power spectral density of noise, N_i, associated with the LOS velocity measured by beam i. Subsequently, the variance of the instrumental

noise, $\sigma^2_{n_i}$, can be derived by multiplying N_i by the Nyquist frequency, f_N, such as (e.g., McMillan and Hay, 2017):

$$\sigma^2_{n_i} = N_i f_N \tag{4}$$

2.4.2 Autocorrelation function method

An alternative method for computing the variance of the instrumental noise involves the calculation of the auto-correlation function (ACF) of the squared LOS velocity time series, as proposed by Lenschow et al. (2000). The ACF quantifies the similarity between a signal and its time-shifted versions across various time lags. This measure provides insight into how much of the signal correlates with its past values, which is essential for distinguishing between the noise and signal components.

~~The characterization requires the identification of the inertial subrange of turbulence, i.e., the range of scales within a turbulent flow where energy cascades from larger to smaller eddies without significant loss to viscosity. In the context of three-dimensional turbulence, the spectrum, $S(k)$, in the inertial subrange is often described by Kolmogorov's -5/3 law and is proportional to $k^{-5/3}$, where k is the wavenumber, inversely proportional to the size of the eddies. This scaling indicates that the energy density decreases with increasing wavenumber (or decreasing eddy size) in a predictable manner. The spectrum, $S_5(k)$, of the vertical velocity measured directly by beam 5 can be related to the dissipation rate as follows:~~

$$S_5(k) = C_w \varepsilon^{2/3} k^{-5/3} + \hat{N}_5$$

~~with $C_w = 0.69$ is the universal Kolmogorov constant (Sreenivasan, 1995; Pope, 2000) and $\hat{N}_5$ the power spectral density of noise in the wavenumber domain.~~ According to Lenschow et al. (2000), after calculating the ACF, the ACF values (excluding the first lag) are fitted to a 2/3 power-law function. This power-law model describes the decay of correlation over time, allowing for the extraction of a coefficient that characterizes how the correlation diminishes as the time lag increases. From this power-law fit, the value of the ACF as the lag tends to zero is estimated by extrapolation of the fitted model. This value is associated with the signal variance.

~~The transition wavelength λ_w between the inertial subrange and the outer scales can be expressed as a function of~~ Subsequently, the ~~integral scale L_w (Eq. **??**) and~~ total variance of the signal is calculated. The instrumental noise variance, $\sigma^2_{n_i}$, is then determined by subtracting the signal variance, as derived from the fitted power-law model, from the total variance. This process enables the separation of the signal and noise contributions to the overall variance. However, this method performs correctly only if the range in which the turbulent cascade occurs is fully captured. This condition is not guaranteed with wind lidar profiler measurements, as the ~~parameter μ:~~

$$\lambda_w = \left[\frac{5}{3} \sqrt{\mu^2 + \frac{6}{5}\mu + 1} - \left(\frac{5}{3}\mu + 1 \right) \right]^{1/2\mu} \frac{2\pi}{C_w} L_w$$

intra-beam effect disturbs the inertial range of turbulence where the cascade takes place.

2.5 Computation of the variance in instrument coordinates

The conventional method for computing variance and standard deviation (the square root of variance) from wind lidar profiler measurements relies on deriving second-order statistics from the reconstructed instantaneous velocity components based on LOS velocities. This approach inherently combines, at each time step, measurements taken at sampling points separated by several tens of meters, depending on the height level of interest. The assumption of instantaneous flow homogeneity (inter-beam effect) introduces an uncertainty in the derived statistics, which is difficult to quantify and can lead to either an overestimation or underestimation of the standard deviation, depending on the frequency and flow configuration. Additionally, this traditional method is affected by both intra-beam filtering and instrumental noise. Crucially, because variance is computed from the reconstructed instantaneous velocity components, it does not account for the noise-induced variance present in the LOS velocity time series which will result in overestimation of variance.

~~Where $\mu = 1.5$ as proposed in several studies (e.g., Lothon et al., 2009; Tonttila et al., 2015; Bodini et al., 2018). These values have been found to provide a good match to most of~~ The combined influence of the inter-beam effect, intra-beam effect, and instrumental noise can result in variance estimates derived from the traditional approach that may appear to align more closely with those derived from a sonic anemometer, but for reasons unrelated to the actual turbulence characteristics. Consequently, the benefits of an increased sampling rate for turbulence measurement using a lidar profiler cannot be accurately assessed with this approach.

The variance method, as referred to in the ~~observed spectra presented in these studies. Following the approach in Tonttila et al. (2015) , one can estimate the timescale, t_w, corresponding to this transition wavelength by dividing λ_w by the collocated wind speed, U. The transition frequency, f_a, between the area of~~ studies (e.g., Stacey et al., 1999a, b; Lu and Lueck, 1999; Rippeth et al., 2002; Guerra , offers an alternative to the traditional approach for computing variance. This method calculates the second-order statistics of the three velocity components by deriving them directly from the second-order statistics of the LOS velocities. Unlike the traditional approach, the ~~outer scales of turbulence and the inertial subrange,~~ variance method is unaffected by the inter-beam effect. However, it is ~~then given by $f_a = 1/t_w$. Finally,~~ still influenced by the intra-beam effect and instrumental noise. Notably, the ~~transition frequency, f_b, between the inertial subrange and the noise-dominated range is set to $f_b \approx 0.8 f_N$, where f_N is the Nyquist frequency. This value of f_b aligns with findings from other studies that identify the noise-contaminated frequency domain in devices using the Doppler effect to measure flow velocity (e.g., Frehlich, 2001; Bodini et al., 2018; Thiébaut et al., 2020b) .~~ impact of instrumental noise can be identified and removed. Hereafter, a hat notation is used to denote standard deviation or variance derived from this method.

~~From Eq. **??**, one can deduce the dissipation rate by invoking Taylor's 'frozen field hypothesis,' which assumes that the turbulence is in a steady state as it advects past the instrument, meaning it is neither developing nor decaying. Under this assumption, one can transform spatial observations into temporal observation, using the relation $f = Uk/2\pi$. The dissipation rate, ε, is thus given by (McMillan and Hay, 2017; Thiébaut et al., 2022):~~

$$\varepsilon = \left(C_w^{-1} \left[S_5(f) \Big|_{f_a}^{f_b} - N_5 \right] f^{5/3} \left(\frac{2\pi}{U} \right)^{5/3} \right)^{3/2}$$

This equation applies under the assumption that the inertial subrange follows the classic -5/3 slope. Computing the dissipation rate from the vertical velocity measured directly by beam 5 The variance method enables the calculation of the variances, $\hat{\sigma}_x^2$ and $\hat{\sigma}_y^2$ of the WindCube v2.1 lidar involves a two-step process. The first step is to determine the power spectral density of $S_5(f)$ between frequencies f_a velocity components u_x and f_b. For this step, it is recommended to fit the measured velocity spectrum using Eq. 2 with $\beta = 5/3$. However, it will be demonstrated in this paper that setting β to this specific value has shown difficulties in accurately representing noise (see Section 3.3). Therefore, it is advisable to set $N_5 = 0$ for the computation of the mean power spectral density. In the second step, the power spectral density of noise, N_5, is computed by performing a second fitting where β is allowed to vary freely. This N_5 is then subtracted from the mean spectral density of $S_5(f)$ computed between f_a u_y (in instrument coordinates) as:

$$\hat{\sigma}_x^2 = \frac{1}{2\sin^2\phi}\left(\sigma_{p_3}^2 + \sigma_{p_1}^2 - 2\cos^2\phi\,\sigma_{p_5}^2\right) \tag{5}$$

$$\hat{\sigma}_y^2 = \frac{1}{2\sin^2\phi}\left(\sigma_{p_2}^2 + \sigma_{p_4}^2 - 2\cos^2\phi\,\sigma_{p_5}^2\right) \tag{6}$$

where $\sigma_{p_i}^2 = \sigma_{b_i}^2 - \sigma_{u_i}^2$ (Eq. 3), is the variance of the LOS velocity recorded by beam i, corrected for the variance of instrumental noise.

In this paper, we restrict the application of the variance method to situations where the wind aligns with a single pair of opposite beams (either pair 1-3 or pair 2-4) of the lidar profilers. This alignment condition was met in 17.1% of the cases. Under these conditions, it can be reasonably assumed that the covariance term, $\hat{\sigma}_{uv}$ (where v represents the cross-wind velocity), which corresponds to $\hat{\sigma}_{xy}$ in this specific condition, is negligible (e.g., Newman et al., 2016). Specifically, when the wind aligns with beams 1 and f_b in the first step. This approach ensures that N_5 accurately represents noise contributions while allowing flexibility in β during the fitting process.

3 Results

3, we have $\hat{\sigma}_u^2 = \hat{\sigma}_x^2$. Conversely, when the wind aligns with beams 2 and 4, it follows that $\hat{\sigma}_u^2 = \hat{\sigma}_y^2$. For brevity, we use $\hat{\sigma}^2$ in place of $\hat{\sigma}_u^2$ hereafter. The standard deviation, $\hat{\sigma}$, is then compared to the along-wind standard deviation, σ, which is derived from sonic anemometer measurements.

2.1 Data availability Key performance indicators and mean wind speedacceptance criteria

The first step when proposing enhancements to lidar technology is to evaluate their impact on data availability of the wind vector. This evaluation was conducted at each measurement height for both enhancements proposed for the WindCube v2.1 lidar profiler. The reduction of probe length did not impact data availability, which remained close to 100% at each measurement altitude for both the commercial and prototype configurations. However, increasing the sampling rate slightly affected of

our analysis focuses on key performance indicators (KPIs), applied to mean wind statistics such as wind speed, that are the mean differences, slope, or the coefficient of determination (R^2) at reference heights corresponding to sonic anemometer measurements. DNV-GL has defined acceptance criteria (ACs) as "best practice" and "minimum allowable tolerances" These criteria, applied to wind speed, flag any KPIs outside the thresholds as "deviations". Table 1 summarizes the ACs established by DNV-GL, which are tested in this paper for the wind speed KPI.

Additionally, the paper addresses data availability. ~~The commercial configuration showed data availability ranging from 99.7% at the first measurement height to 93.2% at the last measurement height, whereas the prototype configuration showed data availability consistently lower by less than 0.5%.~~

~~Next, the effectiveness of~~ Data availability is defined as the ratio of valid data points returned by the ~~prototype configurations was evaluated by testing their ability to measure wind speed averaged over a 10-minute interval~~lidar to the maximum number of possible points that could be acquired during the test. To pass the ~~"Best Practice" standard, a lidar profiler has to demonstrate~~ test, DNV-GL set the data availability threshold at 90%.

2.2 Error statistics metrics

This paper focuses on turbulence measurements, specifically the standard deviation of wind velocity, obtained from both the commercial and prototype lidars. These measurements are compared to the standard deviation provided by the reference instrument; the sonic anemometer. To assess the accuracy and reliability of the lidar measurements, various error statistics are used. These include Root Mean Square Error (RMSE), which quantifies the average magnitude of errors; Mean Absolute Error (MAE), which calculates the average absolute difference between predicted and observed values; bias, which represents the systematic error between the lidar and reference measurements; the coefficient of determination, R^2, which indicates the proportion of variance in the lidar ~~cannot be certified for mean wind speed measurement.~~

Table 1. Acceptance criteria for KPI of mean wind speed in wind lidar profiler certification.

KPI - Wind speed	Definition	
Difference	Percentage difference in mean wind speeds between lidar and reference over the verification campaign, relative to the campaign mean wind speed~~measurements that differ by no more than ±~~.	< 1~~% from the mean wind speed measured by a reference mea~~
Slope	Slope from single-variable regression, constrained to pass through the origin.	
R^2	Correlation coefficient from single-variable regression.	

Here, the mean wind speed measured by the first prototype lidar involving an increase of sampling rate and the second prototype lidar involving a reduction of the probe length was compared to mean wind speed measured by a commercial lidarserving as reference measurement. The mean relative error and the bias were calculated at each measurement heightmeasurements explained by the reference data; and relative error, which expresses the error as a percentage of the reference measurement. Together, these statistical metrics provide a comprehensive evaluation of the lidar's performance in capturing turbulence characteristics relative to the reference instrument.

3 Results

3.1 Mean wind speed and data availability

The first step in proposing enhancements to lidar technology is to evaluate their impact on mean wind speed measurements. Fig.?? illustrates that an increase in the sampling rate leads to a systematic underestimation of the 4a illustrates that the mean vertical wind speed profiles measured by both configurations are closely aligned. However, the difference between the mean wind speed . This underestimation is nearly constant across different altitudes, averaging 1.3%, which corresponds to a bias of approximately 0.1 m/s. Conversely, reducing the probe length results in a systematic overestimation of the measurements provided by the commercial configuration and the reference measurement (black cross in Fig. 4) at the reference altitude is smaller, amounting to 0.98%, compared to a 1.41% difference for the prototype configuration. These results demonstrate that the commercial configuration closely matches the "best practice" AC criterion for the difference in mean wind speed. This overestimation manifests in two distinct patterns: above 100 m, where the prototype lidar overestimates the mean wind speed by an average of 0.5%, and below 100 m, where a significant overestimation occurs, peaking at over 4% resulting in a bias of 0.2 m/s, observed at the first measurement level, 40 m above the ground. , while the prototype configuration, with a larger difference, only meets the "minimum" criterion (Table 1 and Table 2).

The bias in mean wind speed measurements associated with a reduced probe length is illustrated in Fig. ??. The goal is to identify potential parameters that could influence this high bias at lower altitudes. Fig. ??a shows that wind speed does not influence the bias. Although the lowest wind speed at Moreover, the commercial configuration exhibits data availability

Relative error (a) and bias (b) in mean wind speed measurements of the prototype lidars involving an increase in the sampling rate (solid line) and a reduction in the probe length (dashed line), compared to the mean wind speed measured by a commercial lidar, which serves as the reference measurement.

Table 2. Acceptance criteria for KPI achievement applied on mean wind speed associated with the commercial and prototype configurations: ✓✓denotes "best practice" and ✓indicates "minimum" acceptance, as defined in Table 1.

	Difference	Slope	R^2	Data availability
Commercial configuration	✓✓	✓✓	✓✓	✓✓
Prototype configuration	✓	✓✓	✓✓	✓✓

ranging from 99.5% at the lowest measurement height, i.e., 40 ~~m could explain the high bias (i.e., more than 0.4 m /s), this does not hold, as similar mean wind speeds were measured at higher altitudes with less than half the bias. The carrier-to-noise ratio (CNR), an output data of the lidar, was also investigated as a potential source of bias~~ m above the ground, to 93.0% at the highest, i.e., 200 m above the ground, with an overall vertical average availability of 98.2% (Fig.~~??~~ 4b). ~~Despite the significantly higher bias at 40 m compared to that at 160 m, similar CNR values were recorded at both 40 m and 160 m above the ground.~~ Similarly, the prototype configuration follows this trend, with data availability decreasing with altitude. The prototype achieves a vertical average availability of 97.7%, with a minimum of 92.3% recorded at the highest measurement altitude. The prototype configuration consistently shows data availability that is, on average, 0.5% lower than the commercial configuration at nearly all measurement altitudes. Both lidar configurations exceed the 90% data availability threshold set by DNV-GL.

Fig. 5 presents the linear regression of the 30-minute averaged wind speed measured by both lidar configurations in comparison to the reference instrument. Both the commercial and prototype configurations match the "best practice" criteria, with slope values of 1.0 and R^2 values of 0.9847 for the commercial configuration. The prototype configuration shows values that are 1% lower for the slope and almost similar R^2, but these differences are minimal and still within the acceptable range for "best practice."

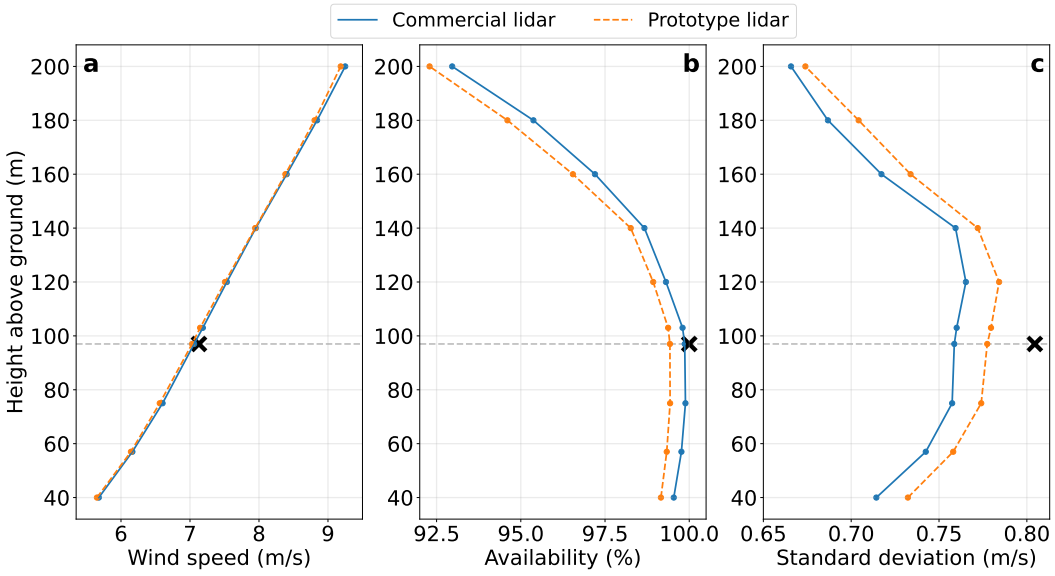

Figure 4. Mean vertical profiles, averaged across the 47-day dataset, of wind speed (a), data availability (b), and standard deviation derived from the variance method (c), measured using the commercial (solid blue curves) and prototype (dashed orange curves) configurations. The black crosses represent the reference measurements from the sonic anemometer, and the grey dashed vertical line marks its position at 97 m above ground.

~~Bias variation in mean wind speed measurement: comparison by mean wind speed (a) and CNR (b).~~

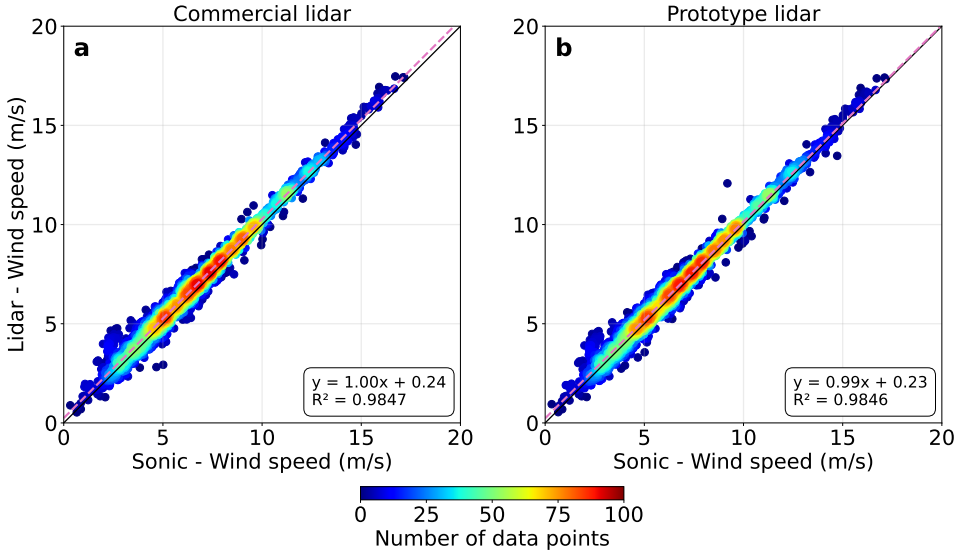

Figure 5. Scatter plots of the 30-minute averaged wind speed measurements over the 47-day campaign, comparing the commercial lidar (a) and prototype lidar (b) with the reference sonic anemometer.

3.2 ~~Standard deviation~~

~~Estimates of the standard deviation measured by the prototype lidars compared to those computed from the commercial lidars are presented in Fig. ??. The regression analysis showed linear relationships with slopes ranging from 0.9 to 1.022 and positive intercepts, all with R^2 values consistently above 0.9. Both the mean and median of the standard deviations were systematically higher for~~

3.2 Impact of sampling rate on turbulence energy capture

The impact of increasing the sampling rate on turbulence measurement can initially be assessed using data from a sonic anemometer, specifically through the computation of along-wind velocity spectra. Integrating these spectra provides the ~~increased sampling rate and reduced probe length configurations. Specifically, the mean standard deviation of the~~ along-wind ~~, cross-wind, and vertical velocities for the increased sampling rate configuration was between 3.5% and 6.3% higher than those from the commercial configuration~~ variance, σ^2. Fig. 6 illustrates the individual spectra and the mean spectrum averaged over the 47-day dataset in both log-log and linear formats. The mean spectrum clearly follows the $f^{-5/3}$ slope, confirming the presence of the energy cascade (Fig. ??6a). ~~For the reduced probe length configuration, the mean standard deviation was between 0.3% (for along-wind velocity) and 3.4% higher (Fig. ??b) . Additionally, the interquartiles of the standard deviation provided by the prototype configurations were consistently higher than those from the commercial configuration, indicating greater variability and sensitivity in the measurements. Furthermore, the vertical evolution of the mean standard deviation showed that both~~

~~Boxplots of the standard deviation of the vertical (σ_5), along-wind (σ_u), and cross-wind (σ_v) velocities for the commercial (blue) and prototype (orange) configurations. Panels (a) and (b) correspond to the studies on increased sampling rate and reduced probe length, respectively. The medians are indicated by green lines, and the means are represented by red diamonds.~~

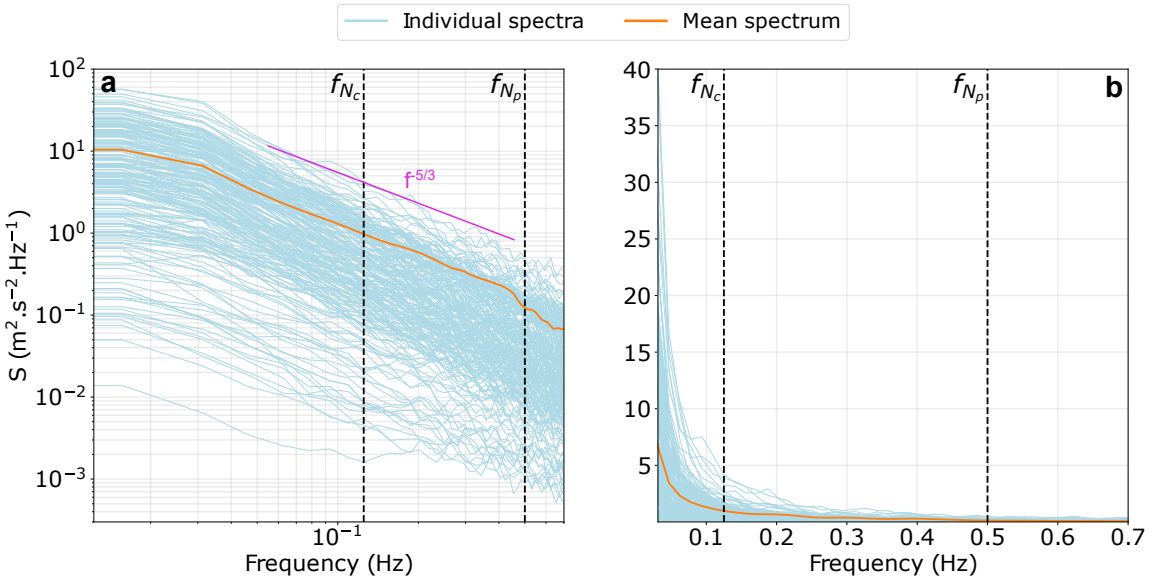

Figure 6. Individual spectra (light blue curves) and mean spectrum (orange curve) measured by the sonic anemometer over the 47-day measurement campaign, presented in log-log (a) and linear (b) formats. Vertical black dashed lines indicate the Nyquist frequencies, f_{N_c} and f_{N_p}, for the commercial and prototype lidar configurations respectively. The pink solid line in panel (a) shows the classic spectral slope $f^{-5/3}$.

~~modifications resulted in higher standard deviations at each altitude, with the discrepancy from the commercial configuration increasing with height (Fig. **??**). Notably, the gaps were more than twice as large at the highest measurement altitude compared to the lowest. Standard deviation, σ, of the along (u), cross (v), and vertical (b_5) velocity components computed from prototype lidar measurements with increased sampling rate (panels a, b, c) and reduced probe length (panels d, e, f) compared to standard deviations derived from commercial lidars measurements.~~

~~Standard deviation, σ, of the along (u), cross (v), and vertical (b_5) wind velocity components computed from prototype lidar measurements with increased sampling rate (panels a, b, c) and reduced probe length (panels d, e, f) compared to standard deviations derived from commercial lidars measurements.~~ The linear representation (Fig. 6b) highlights that most of the energy, associated with larger eddies, is concentrated in the frequency range from 0 to $f_{N_c} = 0.125$ Hz, corresponding to the Nyquist frequency of the LOS velocity in the commercial lidar configuration. However, additional energy, associated with smaller eddies, exists within the range from f_{N_c} to $f_{N_p} = 0.5$ Hz, the latter being the Nyquist frequency of the prototype lidar configuration.

To quantify this effect, the variance was computed by integrating the spectra over two frequency ranges. First, the integration from 0 to f_{N_c} simulated the variance measurable by a sonic anemometer with a sampling rate equivalent to the commercial

lidar. This yielded a mean variance of $0.47\,m^2/s^2$. Second, the integration from 0 to f_{N_p} simulated the variance measurable with a sampling rate equivalent to the prototype lidar, resulting in a mean variance of $0.63\,m^2/s^2$. This comparison indicates that increasing the sampling rate by a factor of 4, relative to the commercial lidar configuration, could capture an additional 34% of the energy associated with smaller eddies. However, this represents the maximum possible improvement, as it is derived from measurements using a sonic anemometer, which is not affected by technical limitations such as the probe length of a wind lidar profiler.

3.3 ~~Velocity~~ LOS velocity spectra

The ~~analysis of LOS velocities obtained from beam 5 involved computational fitting~~ determination of the instrumental noise from the spectral method involves computational fitting of the LOS velocity spectra using a parametric expression (Eq. 2). ~~Various~~ Three weighting schemes were systematically explored to enhance fitting accuracy and minimize errors relative to the measured spectra. ~~Assessing the fitting accuracy included comparing the variance, denoted as σ_5^2, obtained from the integrated fitted spectra with the measured spectra, and calculating their absolute relative differences. Fig. ??~~ Fig. 7a illustrates an example of the three weighting scheme applied to a measured spectrum. This iterative process was conducted across ~~all~~ both lidar configurations, yielding consistent results described hereafter.

The fitted spectra closely matched in the low-frequency domain, approximately up to $f = 0.1$ Hz, but strong divergences were observed thereafter. The low frequencies weighted scheme produced a curve substantially below the measured spectra at higher frequencies, whereas the unweighted scheme yielded a curve slightly above the measured spectra in this frequency range. In contrast, the high frequencies weighted scheme provided a fit that closely matched the measured spectra across all frequencies ~~. The optimal weighting scheme, identified as the high-frequency weighted scheme,~~ and exhibited the lowest mean error. For instance, when applied to the prototype lidar~~with an enhanced sampling rate~~, the mean variance was ~~0.232~~ 0.2321 m^2/s^2 for all

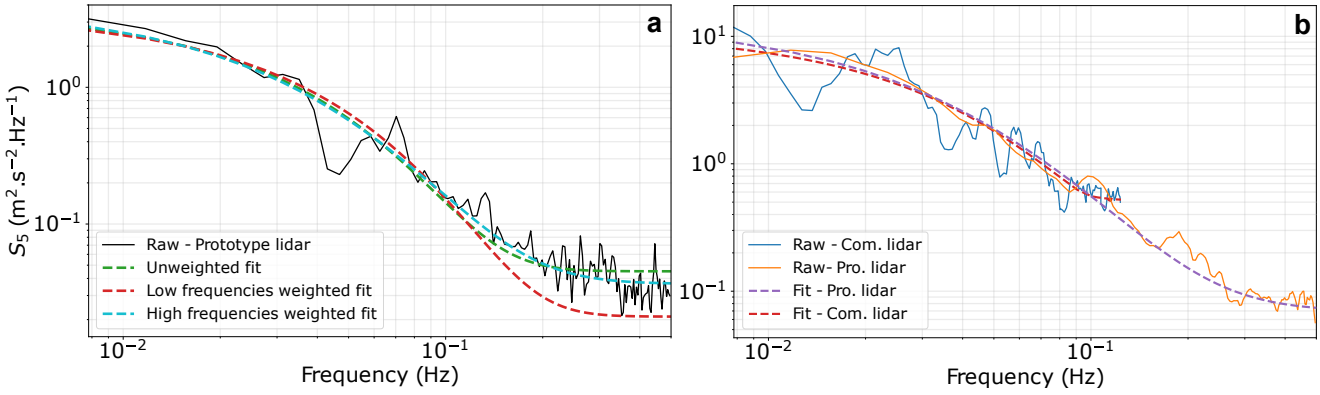

Figure 7. (a) Individual LOS velocity spectrum (solid black) of the prototype lidar fitted with Eq. 2 with three weighted schemes: unweighted fit (dashed green), low frequencies weighted fit (dashed red), and high frequencies weighted fit (dashed blue). (b) Individual LOS velocity spectrum measured by the commercial lidar (blue curve) and prototype lidar (orange curve) fitted with the high frequencies weighted scheme.

integrated fitted spectra using the high-frequency weighted scheme, compared to ~~0.226~~ 0.2262 m^2/s^2 for all integrated measured spectra. This results in an absolute error of 2.6%. Conversely, not employing any weighting during the fitting process resulted in an absolute error between the mean variance nearly three times higher, at 8.5%. Assigning weights to the low frequencies resulted in a mean absolute error exceeding six times that of the high-frequency weighted scheme, at 16.9%. ~~Spectra derived from the commercial configurations and the prototype configuration with a reduced probe length generated absolute errors that were found to be 15-20% higher than the error associated with the configuration using an increased sampling rate, regardless of the weighting scheme used.~~ Thus, the high-frequency weighted scheme was chosen for the fitting. An example of this fitting applied to individual LOS velocity spectra for both the commercial and prototype configurations is shown in Fig. 7b. This weighted scheme enabled the systematic identification of the plateau at higher frequencies, characteristic of white noise. Other weighting schemes did not consistently exhibit this plateau, making it challenging to reliably determine the value of N_i.

3.4 Instrumental noise

3.4.1 Comparison of the spectral and ACF methods

The spectral method yields a median variance that is 1.5 times higher than that of the ACF method for the commercial lidar and twice as high for the prototype lidar (Table 3). While this suggests differences in how each method characterizes noise, the spectral method also results in a mean instrumental noise that is 30-40% lower than that of the ACF method, indicating variations in the way noise is estimated. Moreover, the spread of mean values is notably narrower when using the spectral method, particularly for the commercial lidar, where it is reduced by half compared to the ACF method. This suggests a potential advantage in terms of consistency and stability. Given these observations, we used the spectral method to correct the measured variance, as it appeared to provide more stable estimates of instrumental noise.

3.4.2 Contribution of instrumental noise in the measured LOS velocity variances

This section evaluates, beam by beam, the impact of instrumental noise on the measured LOS velocity variances, which are combined to derive the along-wind variance (Eqs. 5-6). The parametric expression (Eq. 2) used to fit the LOS velocity spectra

~~Individual LOS velocity spectrum (solid black) of the prototype lidar involving an increased sampling rate fitted with Eq. 2 with three weighted schemes: unweighted fit (dashed green), low frequencies weighted fit (dashed red), and high frequencies weighted fit (dashed blue).~~

Table 3. Median and mean (± spread) variance of instrumental noise for commercial and prototype lidars, computed from the LOS velocity measurements across all beams using spectral and ACF methods.

	Commercial lidar		Prototype lidar	
Methods	Spectral	ACF	Spectral	ACF
Median (m^2/s^2)	0.0076	0.0050	0.0129	0.0081
Mean ± spread (m^2/s^2)	0.0108 ± 0.0102	0.0148 ± 0.0228	0.0181 ± 0.0175	0.0237 ± 0.0294

~~Individual LOS velocity spectrum measured by the commercial lidar (blue curve) and prototype lidar (orange curve) with increased sampling rate. The data is fitted using Eq. 2 with $\beta = 19/3$ (a) and $\beta = 5/3$ (b). The fit with $\beta = 19/3$ shows the smallest error.~~

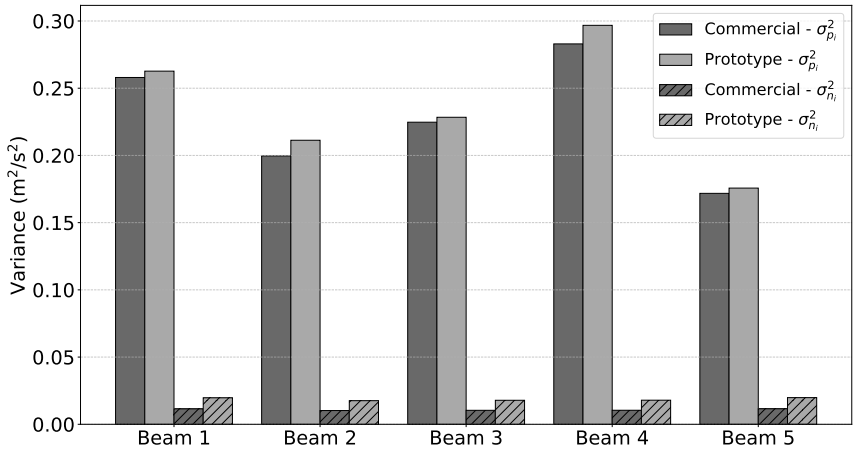

Figure 8. Mean variance of the net contribution from atmospheric turbulence ($\sigma^2_{p_i}$), corrected for instrumental noise derived from the spectral method, measured by each beam i at scales observable by the commercial (dark gray) and prototype (light gray) lidar profilers. Dashed areas represent the mean variance of instrumental noise, $\sigma^2_{n_i}$. The averages were computed over the 47-day dataset.

Table 4. Error Statistics of the along-wind standard deviation derived from the variance method, corrected for instrumental noise, applied on measurements collected by the commercial and prototype lidars in comparison to the reference sonic anemometer.

	Bias (m/~~3. After fitting the spectra using the optimal weighting scheme, we sought instances where this exponent fell within the ra~~
Commercial lidar	-0.0639
Prototype lidar	-0.0466

measured by beam i enables the identification of the power spectral density of instrumental noise, N_i, and the derivation of the variances, $\sigma^2_{n_i}$ (Eq. 4). Fig. 8 compares the mean magnitude of $\sigma^2_{n_i}$ to the mean variance of the net contribution from atmospheric turbulence, $\sigma^2_{p_i}$, corrected for instrumental noise at scales observable by the commercial and prototype lidar profilers.

~~Theoretically, for fully developed turbulence, β in Eq. 2 should be equal to 5~~

~~A general observation, particularly evident in this specific example, is that the fitting of spectra derived from the commercial configuration measurements did not capture the flattened portion of the spectra characteristic of noise. Similar observations were made for fittings applied to spectra from the prototype configuration with a reduced probe length (not shown). However,~~ The mean values of $\sigma^2_{n_i}$, which are nearly identical across all beams, were found to be 0.0108 m^2/s^2 for the commercial configuration (Table 3). A similar trend was observed for the prototype ~~lidar with an increased sampling rate (Fig. **??**a), the flattened portion was clearly reproduced by the fitting. Nonetheless, a general remark is that imposing $\beta = 5$~~configuration, although the mean variance of instrumental noise was 68% higher, at 0.0181 m/~~3 (Fig. **??**b)for the fitting does not generally~~

~~capture the noise portion regardless of the lidar configurations~~^{2} (Table 3). Notably, the contribution of instrumental noise variance to the total variance, σ_b^2, (Eq. 3), was found to be 4.8% and 7.4% for the commercial and prototype lidar configurations, respectively.

~~For measurements performed by the prototype lidar with an enhanced sampling rate, imposing $\beta = 5/3$ during fitting with the optimal scheme resulted in a mean variance of 0.235~~ The mean variances, $\sigma_{p_r}^2$, were consistently higher for measurements obtained with the prototype configuration. Across all beams, the mean value was 0.2288 m^2/s^2, which is ~~3.9%~~ 7.8% higher than the ~~mean variance obtained from integrating the measured spectra. This compares to a 2.6% error when β was not imposed. A similar increase in error when imposing β = 5/3, compared to not imposing it, was also observed in measurements from other lidar configurations . Boxplots of the standard deviation of the spectral power density of noise level, N_5 (a), vertical integral length scale, L_w (b), and dissipation rate, ε (c), for the commercial (blue) and prototype (orange) configurations. The left-hand side of each figure shows results for increased sampling rate, and the right-hand side shows results for reduced probe length.~~

3.5 ~~Noise~~

~~The impact on noise level from modifying the WindCube lidar profiler technology, in terms of sampling rate and probe length, has been evaluated by computing the interquartile ranges and mean. Fig. ??a shows that increasing the sampling rate significantly reduces both the interquartile ranges and the mean noise level compared to the commercial configuration.~~ corresponding mean value for the commercial lidar measurements.

3.5 Along-wind standard deviation

Fig. 9 presents scatter plots of the along-wind standard deviation, $\hat{\sigma}$, derived from the variance method applied on measurements of both lidar configurations compared to the standard deviation, σ, obtained from the reference sonic anemometer. The prototype configuration ~~achieves a median noise level that is 2.3 times lower than~~ demonstrates superior performance across all error metrics, with bias, MAE, and RMSE approximately 25% lower than those of the commercial configuration (Table 4). Additionally, the ~~commercial version, while the mean noise level is 4 times lower due to the high noise values within the upper 75% interquartile range. Conversely, reducing the probe length increases the mean and interquartiles of noise level by a factor of 1.2.~~

3.6 ~~Integral length scale~~

~~A similar analysis was performed on the vertical integral length scale. Fig. ??b shows that reducing the probe length has minimal impact on the computation of~~ coefficient of determination is 5% higher. There is also a reduction in the relative error of the mean standard deviation, with the prototype configuration showing values of 5.7% compared to 7.8% for the commercial configuration.

Fig. 10 presents bin-averaged estimates of $\hat{\sigma}$ compared to estimates of σ (black curve) as a function of binned-averaged wind speed. For all wind speeds, the standard deviation measured by the sonic anemometer consistently remains higher than that

derived from both lidar configurations. Below wind speed of 8 m/s, the standard deviation values from both lidar configurations closely match each other. Within this wind speed range, the standard deviation associated with the integral length scale, with mean and median values differing by less than 1% compared to the commercial commercial lidar is 2.7% higher than that from the prototype configuration. However, above this wind speed threshold, the standard deviation associated with the prototype configuration increases more rapidly with wind speed compared to the commercial lidar. In this wind speed range, the prototype configuration slightly reduces the upper 75% interquartile range and above. Increasing the sampling rate, however, does affect the integral length scale computation. The prototype lidar shows mean and median values that are 7% and 5% lowerstandard deviation associated with the prototype lidar is 13.0% higher than that associated with the commercial configuration. For all wind speed ranges, the prototype lidar measurements exhibited a mean standard deviation and variance that were 2.9% and 7.2% higher, respectively, than those given by of the commercial configuration. Overall, all interquartile ranges were found to be lower with the prototype configuration.

3.6 Dissipation rate

Finally, the impact of modifying the WindCube lidar profiler technology on dissipation rate has been assessed. The dissipation rate was derived from Eq. **??** using spectra fitted with β = 5/3 (Eq. 2). However, this equation is only valid when turbulence is fully developed, i.e., when β is higher than 1 (e.g., Neuhaus et al., 2023). Example of individual spectra derived from the prototype configuration enhancing an increased sampling rate can be found in Fig. **??** for different values of β and thus different turbulent regimes. Spectra with a β value lower than 1 were excluded from the analysis, resulting in the rejection of 3.4% and 3.1% of the spectra for the experiments with increased sampling rate and reduced probe length, respectively. The rejected spectra were associated with mean wind speed not exceeded 5.1 m/s.

The dissipation rate was computed by considering the power spectral density of noise , N_5, resulting from fitting spectra with β as a free parameter, as fixing β = 5/3 often failed to properly identify the flat portion characteristic of noise in the spectra. Neglecting the noise led to dissipation rate values that were, on average, 26% higher . Fig. **??**c illustrates that increasing the sampling rate resulted in a mean dissipation rate increase by a factor of 3.7 and a median increase by a factor of 4, while reducing the probe length led to a mean dissipation rate increase by a factor of 1.2 and a median increase by a factor of 1.5.

4 Discussion

4.1 Impact of increased sampling rate

The increased sampling rate in the modified lidar resulted in a systematic and slight reduction in data availability for the wind vector and a slight underestimation of mean wind speed. The reduction in data availability cannot be conclusively attributed to When proposing an increase in sampling rate to capture smaller eddies and their associated energy through variance, it is essential to assess the instrumental noise and its variance to ensure that the observed changes are due to physical phenomena rather than noise. In this study, we estimate noise-induced variance using two distinct methods. For both lidar configurations,

the mean variances of instrumental noise computed from two methods were found to be consistent with values obtained in previous studies, such as the WindCube lidar analysis by Mann et al. (2009). This alignment reinforces confidence in our estimates.

The increased sampling rate leads to higher instrumental noise compared to the commercial configuration, as expected, since the noise variance is inversely proportional to the number of transmitted pulses (Pearson et al., 2009). In the prototype lidar, achieving a higher sampling rate required reducing the number of pulses leading to the elevated noise levels. The noise variance was approximately 5% of the total variance for the commercial configuration and over 7% for the prototype configuration. While the noise contribution is relatively low, it is not negligible, and its impact should be considered when calculating second-order statistics of LOS velocities in pulsed wind lidar profilers.

Compared to estimates derived from the commercial lidar configuration, the error metrics (bias, MAE, RMSE) of the ~~increased sampling rate and, i.e., reduced accumulation time at each measurement position, as similar magnitudes of reduction could be observed when comparing two commercial configurations. Moreover, although a very slight bias in mean wind speed was found to be relatively constant across different altitudes, it is a positive outcome~~ along-wind standard deviation estimates corrected for instrumental noise using the prototype lidar were notably lower. Additionally, the mean along-wind variance measured by the prototype was higher, suggesting that the increased sampling rate ~~does not significantly impact the measurement of mean wind speed.~~

~~Individual LOS velocity spectra measured by beam 5 of the prototype lidar with an increased sampling rate for different turbulent regimes associated with a β value (Eq. 2).~~

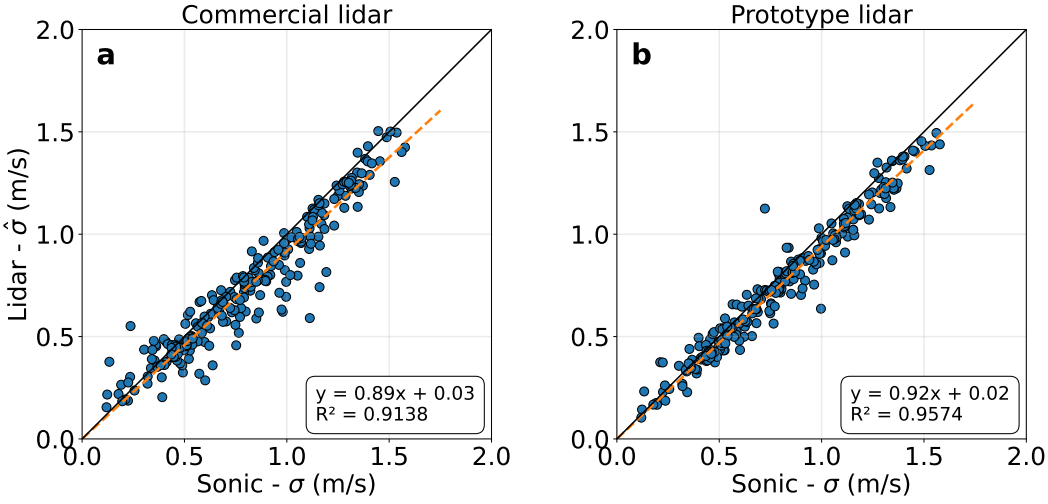

Figure 9. Scatter plots of along-wind standard deviation, $\hat{\sigma}$, derived from the variance method applied on measurements of the commercial and prototype lidar configurations versus standard deviation, σ, derived from the reference sonic anemometer. The standard deviation estimates are restricted to cases where wind direction was aligned with one pair of opposite beams.

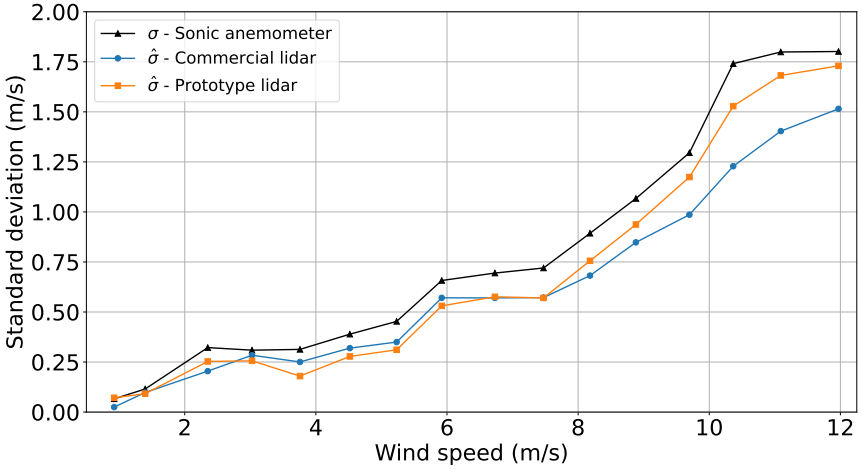

Figure 10. Along-wind standard deviation, $\hat{\sigma}$, derived from measurements of the commercial lidar (blue curve) and prototype lidar (orange curve), compared to the standard deviation, σ, obtained from reference sonic anemometer measurements (black curve) as a function of wind speed.

635 ~~In terms of turbulence measurement,~~ allows for improved detection of turbulent energy associated with smaller eddies. However, this observed improvement remains significantly below the theoretical benefit expected from increasing the LOS sampling rate, as determined through sonic anemometer measurements. The measurement volume of a sonic anemometer is effectively point-like, in comparison to the much larger probe length of wind lidar profilers. The anemometer is in fact essentially free of the ~~increased sampling rateconfiguration improved the overall accuracy of turbulence metrics. The prototype~~ 640 ~~configuration showed higher standard deviations for along-wind, cross-wind, and vertical wind velocities compared to the commercial configuration. This suggests a greater sensitivity to smaller-scale fluctuations, potentially providing a more detailed representation of turbulence.~~ intra-beam effect, which enables it to capture the wind signature of very small eddies.

~~Noise levels were significantly reduced with the increased sampling rate. This reduction in noise can be attributed to the redistribution of noise along an extended frequency range, which allows for clearer differentiation between actual wind~~ 645 ~~fluctuations and measurement noise. A reduction in noise level can improve the reliability of detecting true turbulent fluctuations, thus enhancing the precision of turbulence measurements. The decrease in noise is a beneficial outcome, as it enhances the quality of the data collected, making it easier to distinguish between genuine turbulence and artifacts caused by noise~~One way to mitigate the impact of the intra-beam effect is by significantly reducing the probe length. A shorter probe length would minimize spatial averaging, enhancing the resolution of high-frequency fluctuations in the wind field. However, this reduction 650 is likely to weaken the lidar echo strength, potentially increasing measurement errors. Therefore, a balance must be struck between improving resolution and maintaining signal quality.

The increased sampling rate ~~also affected the integral length scale computation. The prototype lidar with an increased sampling rate showed mean and median values for the integral length scale that were lower than those given by the commercial~~

~~configuration . The frequency associated with the integral length scale is linked to the peak of the energy spectrum or the frequency at which a significant portion of the energy is contained. A too-low sampling rate might fail to identify this frequency, thereby missing the associated eddies. Consequently, for the commercial configuration, the integral length scale is likely sometimes overestimated, as the real energy peak might not be captured, resulting in integral length scale values that do not accurately represent the true turbulence scale. Increasing the sampling rate with the prototype configuration will reduce the number of cases where this peak is not identified. However, it does not guarantee that the new sampling rate will always capture the part of the spectrum with the most energy. Nonetheless, it is likely to provide values closer to reality compared to the commercial lidar configuration.~~

~~The increased sampling rate also demonstrated an improvement in fitting velocity spectra with a parametric expression. The error, computed in terms of variance derived from the measured spectra and associated fitted spectra, was found to be up to 20% lower than that of the commercial configurations and the~~ of the prototype configuration ~~with a reduced probe length. This improvement directly impacts the calculation of~~ could positively impact metrics such as turbulence intensity (TI), which is a key factor due to its influence on structural loads and turbine lifespan. As demonstrated in Fig. 10, this effect is expected to be more pronounced at higher wind speeds, such as at 15 m/s. At this wind speed, TI - referred to as TI15 - is used in design turbulence calculations to define characteristic standard deviation bands, which are essential for classifying turbines according to wind turbulence, as outlined in IEC 61400-1.

Moreover, the ~~dissipation rate deduced from the fitted spectra .~~ increased sampling rate extends the LOS velocity spectra over the frequency domain. This is particularly valuable for floating lidar systems, where measurements are used to derive TI through motion-compensation algorithms which is an ongoing research topic (e.g., Kelberlau et al., 2020; Désert et al., 2021). The ~~dissipation rate computed from the configuration with the~~ buoy's motion generates energy spikes in the LOS velocity spectra at frequencies corresponding to the wave periods, the buoy's natural period, and their interactions (Thiébaut et al., 2024a). This introduces additional variance, $\sigma^2_{m_r}$, which must be accounted for alongside the three other variance terms that contribute to the total variance, $\sigma^2_{b_r}$, measured by each beam i (Eq. 3). With a Nyquist frequency of f_{N_c} = 0.125 Hz, the commercial configuration can detect motion-induced variance for periods up to 8 seconds, while lower-period motion remains undetectable. In contrast, the prototype configuration presented in this paper, with a Nyquist frequency of f_{N_p} = 0.5 Hz, enables the detection of motion effects for periods as short as 2 seconds. Thus, the prototype configuration may offer an advantage in developing motion-compensation algorithms based on the variance method by improving the derivation of true variance through LOS velocity spectra analysis.

The increased sampling rate ~~was found to be up to four times higher than that derived from~~ resulted in a relatively slight 0.5% reduction in data availability compared to the commercial configuration over the 47-day dataset. While this difference is minimal, it may become more noticeable over longer measurement campaigns, which typically last over a year for wind site characterization. Following the measurement campaign presented in this paper, the prototype configuration was installed in December 2022 on Planier Island in the Mediterranean Sea, where it remains operational. The wind characteristics derived from the full year of 2023 are presented in Thiébaut et al. (2024b), including a detailed analysis of data availability. Encouragingly, up to 160 m above sea level, annual data availability exceeded the 90% threshold considered best practice. Beyond this height,

availability gradually declined, reaching below 70% at 220 m. While this highlights an area for further optimization, the prototype lidar has already demonstrated strong performance at critical measurement heights. ~~This is because the prototype configuration captures an extended inertial subrange, resulting in more accurate values of the dissipation rate.~~

4.1 ~~Impact of reduced probe length~~

~~The reduced probe length did not impact the data availability of the wind vector but led to an overestimation of mean wind speed, with significant bias particularly pronounced at lower altitudes. This overestimation, which peaks at over 4% at 40 m above the ground, indicates that while a shorter probe length may improve the resolution of smaller-scale eddies, it introduces substantial inaccuracies in mean wind speed measurements. This bias does not correlate with wind speed or CNR, suggesting that other factors related to probe length and measurement volume may be influencing these discrepancies.~~

~~In terms of turbulence measurement, the reduced probe length configuration also exhibited higher standard deviations, though to a lesser extent than the increased sampling rate configuration. This points to a potential improved sensitivity to smaller eddies, but with the trade-off of introducing more noise into the measurements. The increased noise levels indicate that while the shorter probe length might enhance the capture of smaller-scale fluctuations, it does so at the cost of increased measurement noise, potentially complicating the interpretation of turbulence data.~~

~~However,~~ Moreover, the prototype configuration performed comparably to the ~~reduced probe length had minimal impact on the integral length scale, with mean and median values differing by less than 1% from the commercial configuration. This lack of impact is expected, as the probe length of the commercial lidar is 23 m and that of~~ commercial setup in terms of mean wind characteristics. While the commercial configuration met the "best practice" threshold for all key performance indicators (KPIs), the prototype also achieved this standard, with the exception of mean wind speed differences, where it met the "minimum acceptance" level within the best practice range. This result is promising, as it confirms that the prototype lidar ~~is 15 m, both of which are much smaller than the integral length scale of the turbulence being measured. Consequently, the modification of the probe length does not affect the measurement of large eddies.~~

~~Reducing the probe length was expected to enhance the representation of the inertial subrange, as the probe length of the commercial and prototype configurations directly influences turbulence length scales within this range. However, it was found that, on average, the slope of the spectra, which is supposed to manifest the energy cascade of the inertial subrange, remained similar for both configurations.~~ meets industry standards while offering opportunities for further refinement. With continued development, the prototype lidar has the potential to further enhance wind resource assessments and support the needs of modern wind energy projects.

5 ~~Conclusion~~Conclusions

This study ~~investigates potential modifications to the WindCube v2.1 lidar profiler - specifically, increased sampling rate and reduced probe length - to enhance turbulence measurement. The findings offer a detailed analysis of how these changes impact~~

various wind measurement aspects, including mean wind speed, standard deviation, velocity spectra, noise level, integral length scale, and dissipation rate.

The prototype highlights both the potential and challenges of enhancing the sampling rate in wind lidar systems, particularly for turbulence measurements and the detection of energy from smaller eddies. The prototype lidar configuration, with an its increased sampling rate, samples four times faster than the commercial configuration. This enhancement improves turbulence measurement without affecting mean wind speed measurement. However, a slight reduction in data availability was observed compared to the commercial configurationdemonstrated advantages in capturing higher-frequency fluctuations in the wind field, leading to more accurate along-wind variance estimates. By resolving smaller eddies, the prototype effectively captured additional turbulent energy that the commercial configuration, with its lower sampling rate, could not detect. This improvement was especially pronounced at higher wind speeds, where the prototype's reduced minimum detectable eddy size provided significant benefits. However, the theoretical gains expected from the increased sampling rate were not fully realized due to inherent measurement limitations within the probe, where spatial and temporal filtering effects constrain turbulence detection at certain scales. Despite this, the reduction is minimal enough to allow for further exploration of increased sampling rates to enhance turbulence measurement. Nonetheless, the potential for further increasing the sampling rate is very limited. The prototype configuration already involves a 70% reduction in accumulation time at each LOS measurement position, and further reductions could significantly impact the accuracy of mean wind statistics, which is the primary objective of wind lidar profiler.

The reduced probe length, which entails a 50% reduction in pulse duration compared to the commercial configuration, did not show similar improvements in turbulence measurement. While improvements in turbulent fluctuations were comparable to those achieved with the increased sampling rate also introduced some trade-offs, including elevated instrumental noise and a slight reduction in data availability. Noise contributions to the total variances were non-negligible and required correction to ensure accurate turbulence statistics. It is worth noting that a configuration similar to the prototype examined in this study could be achieved with a commercial lidar, as manufacturers can program an increased sampling rate , they came at the expense of increased noise levels. This makes it unclear whether the higher standard deviations are due to the energy of smaller eddies or noise. Moreover, the reduced probe length configuration exhibited a high bias in mean wind speed measurement compared to the commercial configuration, which is a significant issue for industrial-scale deployment. However, the data length for the with relative ease. However, users should be aware that implementing such a modification would require validation against a meteorological mast to obtain certification, which could add time and cost to deployment.

Another key consideration is balancing increased sampling rate with reduced probe lengthexperiment might be too short to draw definitive conclusions, necessitating a longer experiment for conclusive results.

Ideally, . Ideally, combining both enhancements would yield the optimal configurationfor the WindCube lidar would involve both an increased sampling rate and a reduced probe length, translating to reduced accumulation time with shorter pulse duration. Unfortunately, such a configuration would likely result in poor data availability and questionable accuracy in , improving both temporal and spatial resolution. In this study, the increased sampling rate proved beneficial for turbulence measurements while maintaining acceptable accuracy for mean wind statistics. Therefore, only one modification can be

effectively implemented in the WindCube lidar, with the increased sampling rate being the most promising for improving turbulence measurement without affecting mean wind speed measurementMeanwhile, the effects of reducing the probe length are currently under investigation. While further research is needed to determine its feasibility in field applications, this approach holds promise for future advancements in wind lidar profiler performance.

Author contributions

MT identified the problematic, performed the analysis and drafted the paper. FD and CB contributed to the development and establishment of the two tailored versions of the WindCube v2.1 proposed in this paper and reviewed the manuscript. FG reviewed the manuscript.

Data and code availability

The data is owned by a private consortium with proprietary rights and confidentiality obligations, precluding its sharing alongside this paper.

Acknowledgments

We would like to acknowledge the team at Vaisala, including Mathias Régnier, Loïc Mahe and Cristina Benzo, for their support in providing and configuring the prototype lidar. We are deeply grateful to Louis Marié (Ifremer) for his valuable insights, which significantly contributed to improving the quality of this work.

Competiting interest

The authors declare that they have no conflict of interest.

Financial support

This work was made possible through the support of France Energies Marines and the French government, managed by the Agence Nationale de la Recherche under the Investissements d'Avenir program, with the reference ANR-10-IEED-0006-34. This work was carried out in the framework of the POWSEIDOM project.

References

Bodini, N., Lundquist, J. K., and Newsom, R. K.: Estimation of turbulence dissipation rate and its variability from sonic anemometer and wind Doppler lidar during the XPIA field campaign, Atmospheric Measurement Techniques, 11, 4291–4308, 2018.

Bodini, N., Lundquist, J. K., Krishnamurthy, R., Pekour, M., Berg, L. K., and Choukulkar, A.: Spatial and temporal variability of turbulence dissipation rate in complex terrain, Atmospheric Chemistry and Physics, 19, 4367–4382, 2019.

Branlard, E., Pedersen, A. T., Mann, J., Angelou, N., Fischer, A., Mikkelsen, T., Harris, M., Slinger, C., and Montes, B. F.: Retrieving wind statistics from average spectrum of continuous-wave lidar, Atmospheric Measurement Techniques, 6, 1673–1683, 2013.

Browning, K. A. and Wexler, R.: The determination of kinematic properties of a wind field using Doppler radar, Journal of Applied meteorology and climatology, 7, 105–113, 1968.

Brugger, P., Träumner, K., and Jung, C.: Evaluation of a procedure to correct spatial averaging in turbulence statistics from a Doppler lidar by comparing time series with an ultrasonic anemometer, Journal of Atmospheric and Oceanic Technology, 33, 2135–2144, 2016.

Doviak, R. J. and Zrnic, D. S.: Doppler Radar & Weather Observations, Courier Corporation, Courier Corporation, 1993.

Durgesh, V., Thomson, J., Richmond, M. C., and Polagye, B. L.: Noise correction of turbulent spectra obtained from acoustic doppler velocimeters, Flow Measurement and Instrumentation, 37, 29–41, 2014.

Désert, T., Knapp, G., and Aubrun, S.: Quantification and correction of wave-induced turbulence intensity bias for a floating lidar system, Remote Sensing, 13, 2973, 2021.

Eberhard, W. L., Cupp, R. E., and Healy, K. R.: Doppler lidar measurement of profiles of turbulence and momentum flux, Journal of Atmospheric and Oceanic Technology, 6, 809–819, 1989.

Frehlich, R.: Estimation of velocity error for Doppler lidar measurements, Journal of Atmospheric and Oceanic Technology, 18, 1628–1639, 2001.

Gal-Chen, T., Xu, M., and Eberhard, W. L.: Estimations of atmospheric boundary layer fluxes and other turbulence parameters from Doppler lidar data, Journal of Geophysical Research: Atmospheres, 97, 18 409–18 423, 1992.

Gargett, A. E., Tejada-Martinez, A. E., and Grosch, C. E.: Measuring turbulent large-eddy structures with an ADCP. Part 2. Horizontal velocity variance, 2009.

Guerra, M. and Thomson, J.: Turbulence Measurements from Five-Beam Acoustic Doppler Current Profilers, Journal of Atmospheric and Oceanic Technology, 34, 1267–1284, 2017.

International Electronical Commission: IEC 61400-12-1. Wind energy generation systems – Part 12-1: Power performance measurements of electricity producing wind turbines. Edition 2.0, 2017.

Kelberlau, F. and Mann, J.: Cross-contamination effect on turbulence spectra from Doppler beam swinging wind lidar, Wind Energy Science, 5, 519–541, 2020.

Kelberlau, F., Neshaug, V., Lønseth, L., Bracchi, T., and Mann, J.: Taking the motion out of floating lidar: Turbulence intensity estimates with a continuous-wave wind lidar, Remote Sensing, 12, 898, 2020.

Kristensen, L., Kirkegaard, P., and Mikkelsen, T.: Determining the velocity fine structure by a laser anemometer with fixed orientation, Danmarks Tekniske Universitet, Risø Nationallaboratoriet for Bæredygtig Energi, 2011.

Kropfli, R. A.: Single Doppler radar measurements of turbulence profiles in the convective boundary layer, Journal of Atmospheric and Oceanic Technology, 3, 305–314, 1986.

Lenschow, D. H., Mann, J., and Kristensen, L.: How long is long enough when measuring fluxes and other turbulence statistics?, Journal of Atmospheric and Oceanic Technology, 11, 661–673, 1994.

Lenschow, D. H., Wulfmeyer, V., and Senff, C.: Measuring second-through fourth-order moments in noisy data, Journal of Atmospheric and Oceanic technology, 17, 1330–1347, 2000.

Lhermitte, R. M.: Note on wind variability with Doppler radar, Journal of Atmospheric Sciences, 19, 343–346, 1962.

Lhermitte, R. M.: Note on the observation of small-scale atmospheric turbulence by Doppler radar techniques, Radio Science, 4, 1241–1246, 1969.

Lothon, M., Lenschow, D. H., and Mayor, S. D.: Doppler lidar measurements of vertical velocity spectra in the convective planetary boundary layer, Boundary-layer meteorology, 132, 205–226, 2009.

Lu, Y. and Lueck, R. G.: Using a broadband ADCP in a tidal channel. Part II: Turbulence, Journal of Atmospheric and Oceanic Technology, 16, 1568–1579, 1999.

Mann, J., Cariou, J.-P., Courtney, M. S., Parmentier, R., Mikkelsen, T., Wagner, R., Lindelow, P., Sjoholm, M., and Enevoldsen, K.: Comparison of 3D turbulence measurements using three staring wind lidars and a sonic anemometer, Meteorologische Zeitschrift, 18, 135, 2009.

Mann, J., Peña, A., Bingöl, F., Wagner, R., and Courtney, M. S.: Lidar scanning of momentum flux in and above the atmospheric surface layer, Journal of Atmospheric and Oceanic Technology, 27, 959–976, 2010.

McMillan, J. M. and Hay, A. E.: Spectral and structure function estimates of turbulence dissipation rates in a high-flow tidal channel using broadband ADCPs, Journal of Atmospheric and Oceanic Technology, 34, 5–20, 2017.

Neuhaus, L., Wächter, M., and Peinke, J.: The fractal turbulent/non-turbulent interface in the atmosphere, Wind Energy Science Discussions, 2023, 1–19, 2023.

Newman, J. F., Klein, P. M., Wharton, S., Sathe, A., Bonin, T. A., Chilson, P. B., and Muschinski, A.: Evaluation of three lidar scanning strategies for turbulence measurements, Atmospheric Measurement Techniques, 9, 1993–2013, 2016.

Olesen, H. R., Larsen, S. E., and Højstrup, J.: Modelling velocity spectra in the lower part of the planetary boundary layer, Boundary-Layer Meteorology, 29, 285–312, 1984.

O'Connor, E. J., Illingworth, A. J., Brooks, I. M., Westbrook, C. D., Hogan, R. J., Davies, F., and Brooks, B. J.: A method for estimating the turbulent kinetic energy dissipation rate from a vertically pointing Doppler lidar, and independent evaluation from balloon-borne in situ measurements, Journal of atmospheric and oceanic technology, 27, 1652–1664, 2010.

Pearson, G., Davies, F., and Collier, C.: An analysis of the performance of the UFAM pulsed Doppler lidar for observing the boundary layer, Journal of Atmospheric and Oceanic Technology, 26, 240–250, 2009.

Peña, A., Hasager, C. B., Gryning, S., Courtney, M., Antoniou, I., and Mikkelsen, T.: Offshore wind profiling using light detection and ranging measurements, Wind Energy, 12, 105–124, 2009.

Pope, S. B.: Turbulent flows, Cambridge University Press, 2000.

Richard, J.-B., Thomson, J., Polagye, B., and Bard, J.: Method for identification of doppler noise levels in turbulent flow measurements dedicated to tidal energy, International Journal of Marine Energy, 3, 52–64, 2013.

Rippeth, T. P., Williams, E., and Simpson, J. H.: Reynolds stress and turbulent energy production in a tidal channel, Journal of Physical Oceanography, 32, 1242–1251, 2002.

Sathe, A. and Mann, J.: Measurement of turbulence spectra using scanning pulsed wind lidars, Journal of Geophysical Research: Atmospheres, 117, 2012.

Sathe, A., Mann, J., Gottschall, J., and Courtney, M. S.: Can wind lidars measure turbulence?, Journal of Atmospheric and Oceanic Technology, 28, 853–868, 2011.

Sathe, A., Mann, J., Vasiljevic, N., and Lea, G.: A six-beam method to measure turbulence statistics using ground-based wind lidars, Atmospheric Measurement Techniques, 8, 729–740, 2015.

Sjöholm, M., Mikkelsen, T., Mann, J., Enevoldsen, K., and Courtney, M.: Spatial averaging-effects on turbulence measured by a continuous-wave coherent lidar, Meteorologische Zeitschrift (Berlin), 18, 2009.

Smalikho, I., Köpp, F., and Rahm, S.: Measurement of atmospheric turbulence by 2-μ m Doppler lidar, Journal of Atmospheric and Oceanic Technology, 22, 1733–1747, 2005.

Sreenivasan, K. R.: On the universality of the Kolmogorov constant, Physics of Fluids, 7, 2778–2784, 1995.

Stacey, M. T., Monismith, S. G., and Burau, J. R.: Measurements of Reynolds stress profiles in unstratified tidal flow, Journal of Geophysical Research, 104, 10 935–10 949, 1999a.

Stacey, M. T., Monismith, S. G., and Burau, J. R.: Observations of turbulence in a partially stratified estuary, Journal of Physical Oceanography, 29, 1950–1970, publisher: American Meteorological Society, 1999b.

Strauch, R. G., Merritt, D. A., Moran, K. P., Earnshaw, K. B., and De Kamp, D. V.: The Colorado wind-profiling network, Journal of Atmospheric and Oceanic Technology, 1, 37–49, 1984.

Stull, R. B.: Meteorology for scientists and engineers: a technical companion book with Ahrens' Meteorology Today, 2000.

Teunissen, H. W.: Structure of mean winds and turbulence in the planetary boundary layer over rural terrain, Boundary-Layer Meteorology, 19, 187–221, 1980.

Theriault, K.: Incoherent multibeam Doppler current profiler performance: Part II–Spatial response, IEEE journal of oceanic engineering, 11, 16–25, 1986.

Thiébaut, M., Filipot, J.-F., Maisondieu, C., Damblans, G., Duarte, R., Droniou, E., Chaplain, N., and Guillou, S.: A comprehensive assessment of turbulence at a tidal-stream energy site influenced by wind-generated ocean waves, Energy, 191, 116 550, 2020a.

Thiébaut, M., Filipot, J.-F., Maisondieu, C., Damblans, G., Duarte, R., Droniou, E., and Guillou, S.: Assessing the turbulent kinetic energy budget in an energetic tidal flow from measurements of coupled ADCPs, Philosophical Transactions of the Royal Society A, 378, 20190 496, 2020b.

Thiébaut, M., Quillien, N., Maison, A., Gaborieau, H., Ruiz, N., MacKenzie, S., Connor, G., and Filipot, J.-F.: Investigating the flow dynamics and turbulence at a tidal-stream energy site in a highly energetic estuary, Renewable Energy, 195, 252–262, 2022.

Thiébaut, M., Thebault, N., Le Boulluec, M., Damblans, G., Maisondieu, C., Benzo, C., and Guinot, F.: Experimental Evaluation of the Motion-Induced Effects for Turbulent Fluctuations Measurement on Floating Lidar Systems, Remote Sensing, 16, 1337, 2024a.

Thiébaut, M., Vonta, L., Benzo, C., and Guinot, F.: Characterization of the offshore wind dynamics for wind energy production in the Gulf of Lion, Western Mediterranean Sea, Wind Energy and Engineering Research, 1, 100 002, 2024b.

Thomson, J., Polagye, B., Durgesh, V., and Richmond, M. C.: Measurements of turbulence at two tidal energy sites in Puget Sound, WA, Oceanic Engineering, IEEE Journal of Oceanic Engineering, 37, 363–374, 2012.

Tieleman, H. W.: Universality of velocity spectra, Journal of Wind Engineering and Industrial Aerodynamics, 56, 55–69, 1995.

Tonttila, J., O'Connor, E. J., Hellsten, A., Hirsikko, A., O'Dowd, C., Järvinen, H., and Räisänen, P.: Turbulent structure and scaling of the inertial subrange in a stratocumulus-topped boundary layer observed by a Doppler lidar, Atmospheric chemistry and physics, 15, 5873–5885, 2015.

Tritton, D. J.: Physical fluid dynamics, Springer Science & Business Media, 2012.

Welch, P.: The use of fast Fourier transform for the estimation of power spectra: A method based on time averaging over short, modified periodograms, IEEE Transactions on audio and electroacoustics, 15, 70–73, 1967.

Wildmann, N., Bodini, N., Lundquist, J. K., Bariteau, L., and Wagner, J.: Estimation of turbulence dissipation rate from Doppler wind lidars and in situ instrumentation for the Perdigão 2017 campaign, Atmospheric Measurement Techniques, 12, 6401–6423, 2019.

Wilson, D. A.: Doppler radar studies of boundary layer wind profile and turbulence in snow conditions, 1970.